Comparison of Analytical Theory with Brownian Dynamics Simulations for Small Linear and Circular DNAs

Patrick J. Heath,[†] John A. Gebe,[†] Stuart A. Allison,[‡] and J. Michael Schurr*,[†]

Department of Chemistry, Campus Box 351700, University of Washington, Seattle, Washington 98195-1700, and Department of Chemistry, Georgia State University, Atlanta, Georgia 30303

Received August 8, 1995; Revised Manuscript Received January 2, 1996[⊗]

ABSTRACT: An approximate analytical theory is constructed for the optical anisotropy of a circular weakly bending filament. It is argued that such circles exhibit very nearly *dynamical* mean local cylindrical symmetry, despite their inherent curvature. This theory and the corresponding approximate analytical theory for weakly bending rods are tested by fitting each theory to the results of Brownian dynamics simulations, in which all of the relevant forces are included. A rigorous derivation is presented for the force arising from the torsion potential, which couples torsional strain to writhing and crankshaft motions, and a new more convenient expression is obtained. Simulations of *equilibrium* trajectories performed with and without this force show that it has no significant effect on the optical anisotropy of either circular or linear filaments with parameters appropriate for DNA. However, when large net torsional strains are introduced into planar circles, this force enormously enhances the rate at which twist is converted into writhe during the subsequent *nonequilibrium* trajectories (Chirico, G.; Langowski, J. *Biopolymers* **1994**, *34*, 415−433). The analytical theories give good fits to the simulated anisotropies, and the ratios of best-fit torsion constants to the input values are relatively close to 1.0. These ratios are tabulated as correction factors to be applied to best-fit torsion constants obtained by fitting experimental anisotropy data.

Introduction

Most of our knowledge about the torsion constant between base pairs, or equivalently the torsional rigidity, of DNA comes from fitting approximate analytical theory to experimental time-resolved fluorescence polarization anisotropy (FPA) decays.[1] Indeed, practically all of our information pertaining to the effects of temperature,[2−4] NaCl concentration,[1,5,6] polyamine binding,[1,7] antitumor drug binding,[8] intercalator binding,[9−12] overall base composition,[1,13,14] long-range effects of a $(CG)_8$ sequence,[15] and supercoiling[1,16−19] on the torsion constant is derived from such analyses of time-resolved FPA data. However, alternate methods, that involve ligating equilibrium populations of *small* noncovalently closed *circular* DNAs, yield torsion constants for $N \leq 250$ base pairs (bp) that are about 50% larger than those typically derived from FPA data on *linear* DNAs,[20−22] but for $N \geq 350$ bp yield comparable torsion constants.[6] The possibility that bending a small DNA ($N \leq 250$ bp) into a circle might substantially increase its torsion constant was recently tested by means of time-resolved FPA measurements on both the linear and covalently closed circular forms of the same 181 bp DNA.[23,24] The conclusion of that work, which will be reported elsewhere, rests heavily upon the validity of the analytical theories employed to analyze the data for both the linear and circular species. The primary objective of the present work is to develop suitable analytical theory for the simultaneous twisting and bending of circular DNAs, so that circular and linear DNAs are treated on the same footing, and then to perform a critical test of how well these approximate analytical theories actually fit the results of Brownian dynamics simulations in which all of the relevant forces are taken into account.

Until the recent work of Chirico and Langowski,[25] the *forces*, but not the torques, arising from the torsion potential had generally been omitted from Brownian dynamics simulations. Those authors obtained an expression for that force and showed that it enormously enhanced the rate at which a large net twist initially stored in a planar circle was converted into writhe. The question arises whether those forces also significantly affect the rotational dynamics of the molecule along "equilibrium" trajectories, where the vast majority of departures from the minimum energy geometry are not nearly so large. Indeed, current analytical theories are based on the assumption that the effects of such forces are negligibly small for equilibrium trajectories. A second objective of the present work is to determine the effects of these forces arising from the torsion potential by comparing Brownian dynamics simulations of the equilibrium trajectories of small linear and circular DNAs in the presence and absence of such forces. As will be seen, the results amply justify the neglect of such forces in treating the rotational dynamics along equilibrium trajectories.

As noted by Chirico and Langowski,[25] their treatment of the force arising from the torsion potential was not entirely satisfactory. A third objective of the present work is to complete a rigorous derivation of that force. In the process, substantial clarification of certain troublesome points is achieved, and a simpler expression of greater computational convenience is obtained, which is nevertheless fully equivalent to that of Chirico and Langowski.

An alternative Langevin dynamics method for simulating linear and circular DNAs was recently proposed by Schlick and Olson.[26] In its present form, this method is unsuitable for quantitative simulations of DNA dynamics on Brownian time scales, namely, $t \geq 50$ ps, for several reasons, both practical and fundamental. (1) The force field is altogether inadequate, because it omits true solvent friction on the chain, as well as all hydrodynamic interactions between different parts of the chain. This has the consequence that the predicted

[†] University of Washington.
[‡] Georgia State University.
[⊗] Abstract published in *Advance ACS Abstracts,* April 1, 1996.

S0024-9297(95)01167-3 CCC: $12.00

DNA motions are all largely underdamped and oscillatory in nature. Indeed, the simulations of Schlick and Olson yield periodic oscillations in all properties examined out to times as long as 500 ps, which are completely uncharacteristic of DNA dynamics in solution. The available experimental evidence indicates that thermally excited Brownian motions of all molecules, including DNA, in water on a time scale longer than 50 ps are overdamped and exhibit only monotonic decays with no coherent oscillations of any kind. Certainly, the time-resolved fluorescence polarization anisotropy (FPA) of ethidium intercalated in DNA exhibits only a monotonic decay with no detectable oscillations in experiments with instrumental widths as small as 35 ps (B. S. Fujimoto, unpublished results). (2) Schlick and Olson note that in their method larger masses "produce considerably smaller global movements". Thus, the results of their method contradict the two most distinctive and characteristic features of the Brownian regime, namely, the overdamped character of the motions and the mass independence of all correlation functions of the spatial and angular coordinates. (3) Uncertainties regarding the appropriate masses to be associated with the control points of the *B*-spline representation of the filament may also produce substantial errors in estimated simulation times. Whether due to this mass uncertainty or to the omission of the true solvent friction, the time scale for the simulated writhing of a 1000 bp initially twisted circular DNA, namely, $t \lesssim (1000) \times (50)$ fs $= 50$ ps, is 10^5 times smaller than the corresponding time scale simulated using Brownian dynamics,[25] which time scale was also confirmed in the present work (data not shown). It is important to note that these same Brownian dynamics protocols with comparable filament parameters yield rather accurate descriptions of the experimentally observed decays of the optical anisotropy (defined below) and the dynamic structure factor. (4) The net torsional strain is assumed to be always uniformly distributed; hence local fluctuations in torsional strain about the uniform value are omitted entirely. This has the consequence that the local torques and forces arising from the torsion potential do not correspond to those along any actual thermal trajectory of a real filament, where the torsional strain is not constrained to be uniform. Although this assumption might allow an approximate simulation of the dynamics of global motions, it will lead to a highly erroneous account of the local dynamics, which are sensed by any small probe attached to the DNA. (5) The validity of the implicit Euler method employed by Schlick and Olson to integrate their Langevin equations of motion, specifically to extend the integration to very long time steps, has been called into question by Wu and Watts.[48] The latter authors performed extensive simulations of several systems in order to compare results of the implicit Euler method with those of conventional molecular dynamics and conventional Langevin dynamics, which were obtained by standard Verlet integration. In the conventional Langevin dynamics, the friction factors are related to the fluctuating Langevin forces by the appropriate fluctuation−dissipation relation. However, the nonsolvent friction employed in the implicit Euler method obeys no such fluctuation−dissipation relation. In the systems that were examined, the implicit Euler method gave rather poor results for both equilibrium distributions and dynamical correlation functions and actually performed worse for longer time steps than the conventional methods. Although the implicit Euler method can be used effectively as an energy minimizer (with sufficient friction), as Schlick and Olson have demonstrated, its validity for dynamics simulations, even for DNA *in vacuo*, must be considered doubtful, as Wu and Watts have shown.

Further development of this Langevin dynamics approach was recently reported by Ramachandran and Schlick.[52,53] The effects of solvent forces on translational motions were taken into account by enforcing a fluctuation−dissipation relation between the translational friction factors and the fluctuating Langevin forces. However, hydrodynamic interactions were still omitted, and the effects of solvent torques on the twisting motions of the DNA around its local symmetry axis were completely neglected. In the original work,[26] these twisting motions were implicitly assumed not to contribute directly to the inertia and kinetic energy of the filament and, in the recent work,[52,53] are further assumed not to participate in fluctuation−dissipation exchanges of torque with the solvent. Trajectories of a 1000 bp DNA were run for a wide range of friction factors, extending from the underdamped to overdamped regimes, in order to determine the friction factor that promotes optimum sampling of the configuration space in a relatively short trajectory with a fixed number of iterations (30 000). This optimum friction factor yields a translational diffusion coefficient (D_T) that is about 700 times larger than the corresponding experimental value. It was proposed to simultaneously "scale" both the friction factor and (mass-scaled) simulation time step (20 ps) upward by a factor of 700, in order to reduce the simulated D_T value into the experimental range. Thus, each time step of the simulation was "calibrated" to be equivalent to 14 ns of real time motion of a diffusing DNA. However, this time step calibration reveals an essential limitation of these simulations. In order to satisfactorily simulate a particular motion by simple Langevin dynamics, the relaxation time, or time step, of the fluctuating force must be at least 20-fold smaller than the time scale of the motion itself. In fact, considerable reorientation of the base pairs due to twisting and bending of a real DNA occurs between 0.5 and 14 ns.[1] Evidently, the time steps of Ramachandran and Schlick are much too long (for stationarity of the forces and torques that are responsible) for these 0.5−14 ns motions, and are generally unsatisfactory for any motions that occur in less than about 280 ns. In order to provide precise dynamical information over the 0.5−120 ns time range that is accessed by time-resolved FPA experiments, the calibrated time step would have to be reduced from 14 ns to 25 ps, a 560-fold decrease. In addition, local twisting coordinates would have to be explicitly treated (i.e., simulated) in order to admit nonuniform twist and incorporate solvent friction on the torsional motions, which provide the bulk of the angular displacements on the 0.5−120 ns time scale. Finally, the number of control points would have to be substantially increased to provide adequate spatial resolution of the bending motions. Thus, the calibrated results of Ramachandran and Schlick[52,53] provide only a rough qualitative and semiquantitative picture of the dynamics of the slowest and largest scale motions of the DNA. Due to the omission of hydrodynamic interactions, their results are not only imprecise, but do not scale properly with DNA size, when the friction factor and time step are held constant. A comparison of the results obtained by implicit Euler and standard verlet integration meth-

ods indicated good agreement with regard to certain properties, including writhe. However, a significant difference in average screened Coulomb potential implies that the two methods do not yield the same distributions of intersegment distances. Clearly, considerable further development of the Schlick−Olson and Ramachandran−Schlick approaches is required in order to treat the Brownian dynamics of DNA *in solution* in a realistic and quantitative manner, especially over the relatively short times accessed in FPA experiments.

The Models

The DNA is modeled by a chain of N identical rigid subunits, each of which has length b and is connected to its neighbors on either end by combined twisting and bending springs. The subunits are labeled sequentially by the index j, $j = 1, 2, \ldots N$. In the circle, the Nth subunit is connected to the first in order to close the loop. The linear filament contains $N - 1$ bond vectors ($\mathbf{b}_j$, $j = 1, \ldots N - 1$) and sets of springs between subunits whereas the circle contains N bond vectors and sets of springs. When analyzing experimental data on real DNAs, it is assumed that the number of subunits is sufficiently large that such differences do not significantly affect the comparatively long wavelength dynamics that are manifested in the optical anisotropy. A coordinate frame (x_j, y_y, z_j) is fixed in each subunit j such that z_j is parallel to $\mathbf{b}_j$, and x_y, y_j are perpendicular to $\mathbf{b}_j$. The chromophore is assumed to be part of a particular subunit, for example, the jth, so its rotations reflect those of the jth subunit. Of course, any additional rotations of the chromophore within its confining potential in that subunit are superposed upon the subunit motion.[1,27]

For any chromophore attached to a molecule in a fluid with an isotropic equilibrium state, the optical anisotropy is given by[1,28]

$$r(t) = (^2/_5)\langle P_2(\hat{\mathbf{u}}(0)\cdot\hat{\mathbf{u}}(t))\rangle \tag{1}$$

where $\hat{\mathbf{u}}(t)$ is the instantaneous unit vector along the transition dipole of the chromophore, which is here assumed to be the same for both absorption and emission events. The ensemble average in eq 1 can be replaced by the appropriate average over all possible "initial" times along a temporal trajectory of the "equilibrium" system. Indeed, $r(t)$ is actually evaluated in this manner from the succession of configurations along a Brownian dynamics trajectory, as described below.

The potential energy of the simulated model filament consists of bending (U_b), torsion (U_t), stretching (U_s), and excluded volume (U_{ex}) terms, as described in Appendix A, where convenient expressions for the forces and torques resulting from these potentials are presented and/or derived. Of particular interest here are the *forces* arising from the torsion potential, which vanish for straight filaments, but cause *bent* segments to writhe in the presence of uniform torsional strain, and to undergo crankshaft motions in the presence of nonuniform torsional strain. By performing simulations in the presence and absence of this force, its effects on the dynamics can be ascertained, as described subsequently. The present derivation of this force improves on the earlier derivation of Chirico and Langowski[25] in three main respects. First, the question of which variables constitute a proper set of *independent* coordinates for the Brownian dynamics algorithm is clearly answered. As shown by Chirico and Langowski,[25] the infinitesimal subunit z-axis rotations $\{\delta R_{zj}, j = 1, \ldots N\}$ are neither necessarily nor automatically independent of the infinitesimal subunit translations $\{\delta\mathbf{r}_j, j = 1, \ldots N\}$. The independence of such coordinates was simply assumed in that work. In fact, the infinitesimal z-axis rotations are independent of the infinitesimal translations *only* when the rotations of the subunit coordinate frames *in response to such translations* are carried out in such a way that $\{\delta R_{zj} = 0, j = 1, \ldots N\}$ as is done in the present work. Second, the constraints $\{\delta R_{zj} = 0, j = 1, \ldots N\}$ are explicitly enforced here from the outset when calclating the gradient of U_t with respect to the $\{\delta\mathbf{r}_j, j = 1, \ldots N\}$, in contrast to the *implicit* imposition of the same constraint in the final step of the gradient calculation by Chirico and Langowski. Third, the present derivation yields a much simpler and considerably more computationally convenient expression for these forces, which is nevertheless completely equivalent to that of Chirico and Langowski.

The analytical theory is based on the time-average cylindrical symmetry (or near symmetry) of the underlying *dynamics*.[1,28] The linear filament exhibits mean *local* cylindrical symmetry, such that $\langle\Delta_{xj}(t)^2\rangle = \langle\Delta_{yj}(t)^2\rangle$, where $\langle\Delta_{xj}(t)^2\rangle$ and $\langle\Delta_{yj}(t)^2\rangle$ are the mean-squared angular displacements of the jth subunit around its body-fixed x_j- and y_j-axes, respectively, in time t. For any filament that satisfies this condition and at the same time moves in a solution with an isotropic equilibrium state, the optical anisotropy of a chromophore *attached to the jth subunit* is given by[1,28]

$$\begin{aligned} r_j(t) &= 4\pi\langle Y^*_{20}(\Omega_j(0))\ Y_{20}(\Omega_j(t))\rangle \\ &= (^2/_5)\sum_{n=0}^{2} I_n(t)\ F_n(t)\ C_n(t) \end{aligned} \tag{2}$$

where $\Omega_j(t)$ is the instantaneous solid angle orientation of the transition dipole of the chromophore in the laboratory frame. The twisting correlation function is given by[1,28]

$$C_n(t) = \exp[-n^2\ \langle\Delta_{zj}(t)^2\rangle/2] \tag{3}$$

and the tumbling correlation function is given by[1,28]

$$F_n(t) = \exp[-(6 - n^2)\langle\Delta_{xj}(t)^2\rangle/2] \tag{4}$$

where $\langle\Delta_{zj}(t)^2\rangle$ is the mean-squared angular displacement of the jth subunit around its z_j-axis. The internal correlation functions, $I_n(t)$, depend on the orientation of the transition dipole within the subunit and also reflect any rapid local motions of the chromophore with respect to the subunit frame. In the present test of analytical formulas against Brownian dynamics simulations, the chromophore transition dipole is assumed to be completely immobile with respect to the subunit. In that case, the I_n are given by the well-known trigometric expressions:[1,28] $I_0 = ((^3/_2)\cos^2(\epsilon_0) - {}^1/_2)^2$; $I_1 = 3\cos^2(\epsilon_0)\sin^2(\epsilon_0)$; $I_2 = (^3/_4)\sin^4\epsilon_0$; where ϵ_0 is the polar angle between the local symmetry axis, z_j, and the transition dipole.

Theoretical arguments presented in Appendix B indicate that the circular chain also exhibits dynamical mean *local* cylindrical symmetry to a satisfactory level of approximation. For the circular chain all subunits are equivalent. It is shown in Appendix B that, for the $j = 1$ subunit, $\langle\Delta_{x1}(t)^2\rangle \cong \langle\Delta_{y1}(t)^2\rangle$, provided two conditions are met. First it is required that $D_{\|} = D_{\perp}$, where

$D_{\|}$ and $D_{\perp}$ are the diffusion coefficients for uniform (rigid-body) rotation of the circle around its own symmetry and transverse axes, respectively. For the circular model filament considered here, this condition ($D_{\|} \cong D_{\perp}$) is very nearly satisfied. Second, it is required that in-plane bending of the circle makes nearly the same contribution to the mean-squared angular displacement of $\mathbf{b}_1$ around its transverse out-of-plane y_1-axis as does out-of-plane bending to the mean-squared angular displacement of $\mathbf{b}_1$ around its transverse in-plane x_1-axis, as shown in Appendix B. Under these conditions, then, $\langle \Delta_{x1}(t)^2 \rangle \cong \langle \Delta_{y1}(t)^2 \rangle$, and eqs 2−4 apply, despite the persistent bend of the line of local z_j-axes of the subunits comprising the circle.

In the analytical theory, the stretching and excluded volume potentials are omitted. The actual DNA is highly inextensible, so the stretching force constant should be quite large and the effects of stretching quite small in that case. For the short chains considered here, when the linking difference (defined below) vanishes, there is no significant overlap of "excluded" volumes even in the absence of excluded volume forces. Consequently, those forces also should have no significant effect on the dynamics. Of potentially greater significance is the fact that the *forces* (but not the torques) arising from the torsion potential are also omitted from the analytical theory. The validity of that approximation can be judged from the results of Brownian dynamics trajectories run in the presence and absence of such forces, which reveal no significant effects of those forces in either the linear or circular DNAs *at equilibrium*, as will be shown. Thus, in the analytical theory the direct forces that act to translate the subunits arise exclusively from the bending potential, which governs $\langle \Delta_{yj}(t)^2 \rangle$, whereas the torques that act to rotate the subunits around their own z_j-axes either in the analytical theory or in the simulations arise exclusively from the torsion potential, which governs $\langle \Delta_{zj}(t)^2 \rangle$.

The Brownian Dynamics Protocol. The Brownian dynamics procedure is based on the Ermak−McCammon algorithm,[29] as adapted to discrete wormlike chains by Allison and co-workers,[30,31] and is similar to that described previously.[32] Each Brownian "move" during the time interval Δt consists first of small subunit rotations around their own z_j-axes with no subunit translations, followed by small subunit translations with no subunit rotations around their own z_j-axes. A complete update of the Euler angles that orient each subunit frame in the lab frame is undertaken only after these two half-steps of each Brownian move are completed.

In the first half-step of each Brownian move, the subunit rotations ($\delta R_{zi}(\Delta t)$) around their z_i-axes are determined according to the relation

$$\delta R_{zi}(\Delta t) = D_r\, T_i(t)\, \Delta t/(k_B T) + f_i(\Delta t) \tag{5}$$

wherein $D_r/k_B T = 1/\gamma$ is the mobility, or reciprocal subunit friction factor, for azimuthal rotation around its symmetry axis, and $T_i(t) = g(\phi_{i,i+1} - \phi_{i-1,j})$, where $\phi_{j,j+1} = \alpha_{j,j+1} + \gamma_{j,j+1}$ is the net twist of the Euler rotation from the jth to $(j+1)$th frame (cf. eq A36 in Appendix A). The fluctuating displacement $f_i(t)$ is a small random scalar chosen so that

$$\langle f_i(\Delta t) \rangle = 0, \quad i = 1, \ldots N \tag{6a}$$

$$\langle f_i(\Delta t)\, f_j(\Delta t) \rangle = 2 D_r \Delta t \delta_{ij}, \quad \text{all } i, j \tag{6b}$$

The protocol for generating N random scalars with the requisite mean and covariance was described previously.[32]

After the subunit rotations around their z_i-axes are determined, the unit vectors $\mathbf{f}_i$ along x_i and $\mathbf{v}_i$ along y_i must be updated, subject to the constraint that no subunit positions are changed. This constraint will be satisfied provided the rotations around the subunit x_i- and y_i-axes all vanish, that is, $\{\delta R_{xi} = 0, \delta R_{yi} = 0; i = 1, \ldots N\}$. When only the $\{\delta R_{zi}, i = 1, \ldots n\}$ are nonvanishing, eqs A26 and A27 indicate that

$$\delta \mathbf{f}_i = \delta R_{zi} \mathbf{v}_i \tag{7a}$$

$$\delta \mathbf{v}_i = -\delta R_{zi} \mathbf{f}_i \tag{7b}$$

which are equivalent to the relations employed previously.[32] These small corrections are added to $\mathbf{f}_i$ and $\mathbf{v}_i$, respectively, and the resulting vectors renormalized.

In the second half-step of each Brownian move, the subunit translations are determined according to the relation,

$$\mathbf{r}_i(t + \Delta t) - \mathbf{r}_i(t) = \sum_{j=1}^{N} \mathbf{D}_{ij}(t)\, \mathbf{F}_j(t)\, \Delta t/k_B T + \mathbf{S}_i(\Delta t) \tag{8}$$

wherein $\mathbf{F}_j(t)$ is the total force on the jth subunit, which is given by

$$\mathbf{F}_j(t) = (\mathbf{F}_{ex}(t))_j + (\mathbf{F}_s(t))_j + (\mathbf{F}_b(t))_j + (\mathbf{F}_t(t))_j \tag{9}$$

where $(\mathbf{F}_{ex}(t)_j$ is the force due to the excluded volume potential, which is given in eq A8, $(\mathbf{F}_s(t))_j$ is the force due to the stretching potential, which is given in eq A9, $(\mathbf{F}_b(t))_j$ is the force due to the bending potential, which is given in eqs A12−A14, and $(\mathbf{F}_t(t))_j$ is the force due to the torsion potential, which is given in eqs A33 and A34. The instantaneous mobility tensor is given for nonoverlapping subunits by

$$\mathbf{D}_{ij}/k_B T = \begin{cases} (1/8\pi\eta a)[\mathbf{1} + \hat{\mathbf{r}}_{ij}\hat{\mathbf{r}}_{ij} + 2(a^3/r_{ij}^3)(\mathbf{1}/3 - \hat{\mathbf{r}}_{ij}\hat{\mathbf{r}}_{ij})], & i \neq j \\ \mathbf{1}/6\pi\eta a, & i = j \end{cases} \tag{10a}$$

and for overlapping subunits by

$$\mathbf{D}_{ij}/k_B T = (1/6\pi\eta a)\left[\left(1 - \frac{9}{32}\frac{r_{ij}}{a}\right)\mathbf{1} + \frac{3}{32}\frac{\mathbf{r}_{ij}\mathbf{r}_{ij}}{a r_{ij}}\right] \tag{10b}$$

wherein a is the subunit hydrodynamic radius for translational motion, $\hat{\mathbf{r}}_{ij} = \mathbf{r}_{ij}/|\mathbf{r}_{ij}|$ is a unit vector along $\mathbf{r}_{ij} = \mathbf{r}_i - \mathbf{r}_j$, $\mathbf{1} = \hat{\mathbf{x}}\hat{\mathbf{x}} + \hat{\mathbf{y}}\hat{\mathbf{y}} + \hat{\mathbf{z}}\hat{\mathbf{z}}$ is the unit tensor, and η is the solvent viscosity.[33,34] The fluctuating displacement $\mathbf{S}_i(\Delta t)$ is a small random vector chosen such that

$$\langle \mathbf{S}_i(\Delta t) \rangle = 0, \quad i = 1, \ldots N \tag{11a}$$

$$\langle \mathbf{S}_i(\Delta t)\, \mathbf{S}_j(\Delta t) \rangle = 2\mathbf{D}_{ij}(t)\, \Delta t, \quad \text{all } i, j \tag{11b}$$

The protocol for generating random vectors with the requisite mean and covariance was described previously.[29,35]

After the subunit translations in a given step are determined, the unit vectors $\mathbf{f}_j$, $\mathbf{v}_j$, $\mathbf{u}_j$ along the subunit x_j, y_j, z_j axes, respectively, are updated as follows. The new unit vector, $\mathbf{u}_j(t + \Delta t) = (\mathbf{r}_{ij}(t + \Delta t))/|\mathbf{r}_{ij}(t + \Delta t)|$, and the change, $\delta \mathbf{u}_j = \mathbf{u}_j(t + \Delta t) - \mathbf{u}_j(t)$, are calculated. The changes $\delta \mathbf{u}_j$ are sufficiently small that they are to

first order perpendicular to $\mathbf{u}_j(t)$. When the subunit rotations around their z_j-axes are required to vanish, we have from eqs A26 and A27 that

$$\delta\mathbf{f}_j = -\delta R_{yj}\mathbf{u}_j = -(\delta\mathbf{u}_j\cdot\mathbf{f}_j/|\mathbf{u}_j|)\mathbf{u}_j = -(\delta\mathbf{u}_j\cdot\mathbf{f}_j)\mathbf{u}_j \quad (12a)$$

$$\delta\mathbf{v}_j = \delta R_{xj}\mathbf{u}_j = (-\delta\mathbf{u}_j\cdot\mathbf{v}_j/|\mathbf{u}_j|)\mathbf{u}_j = -(\delta\mathbf{u}_j\cdot\mathbf{v}_j)\mathbf{u}_j \quad (12b)$$

which are equivalent to the corresponding relations employed previously.[25,32] In practice, after $\delta\mathbf{f}_j$ is computed according to eq 12a, it is added to $\mathbf{f}_j$, and the resultant is multiplied (scalar product) by $(\mathbf{1} - \mathbf{u}_j(t + \Delta t)\,\mathbf{u}_j(t + \Delta t))$, to project out any component parallel to $\mathbf{u}_j(t + \Delta t)$, and finally renormalized to obtain $\mathbf{f}_j(t + \Delta t)$. Then the final unit vector is calculated according to $\mathbf{v}_j(t + \Delta t) = \mathbf{u}_j(t + \Delta t) \times \mathbf{f}_j(t + \Delta t)$.

After the unit vectors, $\mathbf{f}_j$, $\mathbf{v}_j$, $\mathbf{u}_j$, and bond lengths, $|\mathbf{b}_j| = |\mathbf{r}_{j,j+1}|$, are determined following each complete Brownian move, the frame-to-frame Euler rotations, $\Phi_{j,j+1} = (\alpha_{j,j+1}\,\beta_{j,j+1}\,\gamma_{j,j+1})$ that orient the frames of the $(j + 1)$th subunits in the frames of the jth subunits are determined according to the relations

$$\beta_{j,j+1} = \arccos(\mathbf{u}_{j+1}\cdot\mathbf{u}_j) \quad (13a)$$

$$\alpha = \begin{cases} \alpha_C, & \text{if } \mathbf{u}_{j+1}\cdot\mathbf{v}_j > 0 \\ -\alpha_C, & \text{if } \mathbf{u}_{j+1}\cdot\mathbf{v}_j < 0 \end{cases} \quad (13b)$$

where $\alpha_C = \arccos(\mathbf{u}_{j+1}\cdot\mathbf{f}_j)/\sin\beta_{j,j+1})$ is the value in the interval $0 \le \alpha \le \pi$ returned by the computer. In addition,

$$\alpha + \gamma = \begin{cases} (\alpha + \gamma)_C, & \text{if } \sin(\alpha + \gamma) > 0 \\ -(\alpha + \gamma)_C, & \text{if } \sin(\alpha + \gamma) < 0 \end{cases} \quad (13c)$$

where $(\alpha + \gamma)_C = \arccos[(\mathbf{f}_i\cdot\mathbf{f}_{i+1} + \mathbf{v}_i\cdot\mathbf{v}_{i+1})/(1 + \mathbf{u}_i\cdot\mathbf{u}_{i+1})]$ is the value in the interval $0 \le \alpha + \gamma \le \pi$ returned by the computer, and $\sin(\alpha + \gamma) = \sin[(\mathbf{f}_i\cdot\mathbf{f}_{i+1} - \mathbf{v}_i\cdot\mathbf{v}_{i+1})/(1 + \mathbf{u}_i\cdot\mathbf{u}_{i+1})]$. The value of γ is determined by the difference, $\gamma = (\alpha + \gamma) - \alpha$.

The calculations presented here were performed using the first-order algorithm outlined above. However, a comparison of the results of both first- and second-order[36] algorithms was made and for the present examples revealed no significant differences either in results or in computational efficiency. The time step employed in the simulations presented here was $\Delta t = 25$ ps.

The Brownian dynamics simulations were checked in several ways. (1) The results were demonstrated to be independent of the size of the time step. (2) The mean potential energies of the twisting, bending, and stretching springs during the simulations were evaluated. After subtracting any contributions from uniform strains, the results were found to match the predicted equipartition values from equilibrium statistical mechanics. (3) For linear DNAs, the distribution of end-to-end distances and the mean squared end-to-end distance during the simulation were determined and shown to closely match those of the initial distribution, which were determined by equilibrium Monte Carlo simulations. (4) For 30-subunit circular DNAs with linking difference, $\Delta l = 3$, the writhes of different configurations during the simulation were computed according to the discretized Gauss integral,[37]

$$w = \frac{1}{4\pi}\sum_{i=1}^{N}\sum_{\substack{j=1 \\ i\neq j}}^{N}(\mathbf{b}_j \times \hat{\mathbf{r}}_{ij}\cdot\mathbf{b}_i)/|\mathbf{r}_{ij}|^2 \quad (14)$$

and averaged. This mean writhe was compared with that obtained by an equilibrium Monte Carlo simulation[38] of a circular chain containing the same number ($N = 30$) of subunits of the same size with the same twisting and bending potential, a hard-cylinder potential with the same diameter σ, fixed bond lengths b, and the same linking difference Δl. For small circles with such modest writhe, the details of the intersubunit repulsive potential are practically without consequence. Very good agreement between the two writhes confirms that the Brownian dynamics simulation yields the correct equilibrium writhe. (5) The excess twist was also calculated for different configurations during the simulation, according to

$$\Delta t = \sum_{j=1}^{N}(\alpha_{j,j+1} + \gamma_{j,j+1} - \phi_0) \quad (15)$$

The sum of the excess twist (Δt) and the writhe (w) was found to remain constant (within significant simulation errors) and in good agreement with the linking difference according to the topological relation,

$$\Delta l = \Delta t + w \quad (16)$$

In fact, $\Delta l = l - l_0$, where l is the integral linking number, or number of turns of one strand around the other, and $l_0 = N\phi_0$ is the intrinsic twist. When the simulation is initiated with a planar configuration, for which $w = 0$, as is the case here, then $(\Delta l)_0 = (\Delta t)_0$ for that initial configuration. It should be noted that eq 15 is never imposed as a constraint during the Brownian dynamics simulation. Instead, its satisfaction is a test of the trigometric manipulations employed during the simulation.

The Analytical Theory. The model treated by the analytical theory differs in three main respects from the model simulated by the Brownian dynamics algorithm. (i) All stretching forces are omitted. In effect, the DNA is assumed to have a fixed contour length. (ii) All intersubunit repulsions are omitted. This is without consequence for such short DNAs with $\Delta l \cong 0$. (iii) The *forces* (as opposed to torques) arising from the torsion potential are omitted. This omission decouples fluctuations in twist from fluctuations in writhe. As shown below, these forces due to the torsion potential have no significant effect on the optical anisotropy decays of either the linear or circular model filaments *at equilibrium*, although they enormously enhance the rate at which a planar circular model filament with nonzero net torsional strain evolves to its equilibrium structure, as shown previously be Chirico and Langowski[25] and confirmed in the present work.

Analytical expressions for $\langle\Delta_{zj}(t)^2\rangle$ for linear[1,28,39] and circular[40] model filaments were given previously. In either case, the results can be expressed as

$$\langle\Delta_{zj}(t)^2\rangle = 2D_z t + 2\sum_{l=2}^{N} Q_{jl}^2 d_l^2(1 - e^{-t/\tau_l}) \quad (17)$$

where D_z is the diffusion coefficient for uniform rotation around the subunit symmetry axis, d_l^2 is the mean-squared amplitude of the lth normal mode, τ_l is the

relaxation time of that same normal mode, and Q_{jl} is the projection of the lth normal mode onto the jth subunit. For linear DNAs,[1,28,29] $D_z = k_B T/N\gamma$, where γ is the subunit friction factor for azimuthal rotation, and

$$d_l^2 = k_B T/(4\alpha \sin^2((l-1)\pi/2N)) \quad (18)$$

$$\tau_l = \gamma/(4\alpha \sin^2((l-1)\pi/2N)) \quad (19)$$

$$Q_{jl}{}^2 = (2/N)\cos^2((j - {}^1/_2)(l-1)\pi/N)$$

For circular DNAs,[40] $D_z = (k_B T/N\gamma) + D_R$, where $D_R = ({}^1/_3)(D_{||} + 2D_\perp)$ is the diffusion coefficient for uniform tumbling of the circle, and

$$d_l{}^2 = k_B T/(4\alpha \sin^2((l-1)\pi/N)) \quad (20)$$

$$\tau_l = \gamma/(4\alpha \sin^2((l-1)\pi/N)) \quad (21)$$

$$Q_{jl}{}^2 = 1/N \quad (22)$$

where α is the torsion constant between subunits. For a circular DNA, D_z must be augmented by $D_\perp \cong D_R$, because both uniform spinning of the DNA around its local z-axis at fixed orientation of the circle and uniform rotation of the circle around an in-plane axis parallel to $\mathbf{b}_j$ contribute as independent Gaussian random processes to increase $\langle \Delta_{zj}(t)^2 \rangle$. Also, for the circular DNA, Q_{jl} and $\langle \Delta_{zj}(t)^2 \rangle$ are independent of the particular subunit j, as expected.

An analytical expression for $\langle \Delta_{xj}(t)^2 \rangle$ was given previously[41] for a linear weakly bending rod, and a corresponding expression for a weakly bending circular filament is derived in Appendix B. In either case, the result can be expressed as

$$\langle \Delta_{xj}(t)^2 \rangle = 2D_R t + 2(b/P)\sum_{l=l_1}^{N}(S_{j+1,l} - S_{jl})^2(1 - e^{-t/T_l}) \quad (23)$$

where $l_1 = 3$ for linear molecules and $l_1 = 2$ for circles, D_R is again the diffusion coefficient for uniform tumbling, b is the fixed rise per subunit, or bond-vector length, $P = \kappa_\beta b/k_B T$ is the persistence length, and S_{jl} is the projection or the lth normal displacement mode onto the jth subunit. By similarity transformation, the matrix **S** diagonalizes the dynamical matrix **HD**, where **D** is the force constant matrix and **H** is the hydrodynamic interaction matrix. That is,

$$(\mathbf{S}^{-1}\,\mathbf{HD}\,\mathbf{S})_{lm} = \Lambda_l \delta_{lm} \quad (24)$$

where the Λ_l, $l = 1, \ldots N$, are eigenvalues of the **HD** matrix. The relaxation time of the lth bending normal mode is given by[41]

$$T_l = fb^3/(k_B T P \Lambda_l) \quad (25)$$

where $f = 6\pi\eta a$ is the friction factor for bead translation, and a is the subunit hydrodynamic radius for translational motion. The Λ_l and S_{jl} are determined numerically from the **HD** matrix using the protocol (and normalization) described previously.[41] Explicit forms for **D** and **H** for linear DNAs were presented previously,[41] and for circular DNAs are presented in Appendix B. The matrix **D** depends only upon N and connectivity. When $a = b/2$, as assumed henceforth, both **H** and **HD** also depend only upon N and connectivity.

Averaging over Subunits. The mean anisotropy was computed by averaging the anisotropies of the individual subunits according to $r(t) = (1/N)\sum_{j=1}^{N} r_j(t)$. This averaging was performed for the Brownian dynamics simulations and was also performed in the analytical theory that was fitted to the simulated data.

Selection of Parameters. For the present tests, we take $N = 21$ subunits and $b = 31.8$ Å, which corresponds to 9.35 bp per subunit. The overall length then corresponds to 196 bp. In treating the tumbling and bending motions, each subunit is regarded as a sphere with hydrodynamic diameter $2a = b = 31.8$ Å. In the case of small linear DNAs, contiguous spheres of this size are known to give D_R values in good agreement with those measured for real DNAs with the same contour length, and also with those calculated for completely rigid cylinders with the same contour length and a 12.5 Å radius by the theory of Tirado and Garcia de la Torre.[42,43] However, in treating azimuthal rotation around its local symmetry axis, each subunit is regarded not as a sphere, but as a cylinder with a hydrodynamic radius $r_{cyl} = 12$ Å, and its friction factor is taken to be $\gamma = 4\eta b\pi r_{cyl}{}^2 = 5.75 \times 10^{-22}$ dyne cm s. This value of the hydrodynamic cylinder radius was measured for DNAs containing 43−69 bp.[44,51] The temperature is $T = 293$ K, and the solvent viscosity is $\eta = 0.01$ P, corresponding to water at 20 °C. The bending constant κ_β is chosen to give our current best guess for the dynamic persistence length, $P = 1500$ Å.[1,14] The angle between the transition dipole and the local z-axis is $\epsilon_0 = 71.5°$, which is within the acceptable range.[1,27]

In the Brownian dynamics simulations, the stretching force constant is taken as $q = 1000\ k_B T/b_0{}^2 = 400$ dyne cm^{-1}. The parameters of the repulsive Lennard-Jones potential are $\sigma = 35$ Å and $\epsilon = 0.0385 k_B T = 1.56 \times 10^{-15}$ dyne cm. In addition, the linking difference is taken to be $\Delta l = 0$.

In the analytical theory the value of the uniform rotational diffusion coefficient for the linear model filament is taken to be $D_R = 4.34 \times 10^5$ s^{-1}. Counting the half-subunits at both ends, the linear filament has an effective contour length, $L = (21)(31.8) = 668$ Å, which corresponds to 196 base pairs, as noted above. This D_R value was obtained by interpolating the experimental data of Elias and Eden[45] to 196 base pairs, and then scaling by (293/277)(0.016/0.01) to 20, w conditions. This experimental value is believed to be the best available estimate of D_R for the equilibrium ensemble of variously bent chains. Analysis of the simulated data were also performed using a 10% smaller value of D_R, which caused less than a 1% change in the best-fit α values. For the circular model, the value of the uniform rotational diffusion coefficient is taken to be $D_R = 2.07 \times 10^5$ s^{-1}. This value is calculated according to $D_R = ({}^1/_3)(D_{||} + 2D_\perp)$, wherein $D_{||} = 1.98 \times 10^5$ s^{-1} and $D_\perp = 2.12 \times 10^5$ s^{-1} are calculated using the theoretical expressions of Yamakawa and Yamaki.[46] The ratio $D_{||}/D_\perp = 1.07$ is sufficiently close to 1.0 that the assumption of mean local cylindrical symmetry is approximately obeyed in this regard.

Simulations of the optical anisotropy were performed for several values of the torsion constant α. For purposes of comparison, the actual torsion constant between the present subunits (α_0) is converted to the equivalent torsion constant between base pairs that yields the same torsional rigidity, that is, $\alpha = (31.8/$

3.4)α_0. Simulations were performed for $\alpha = 2$, 3, 4, 5, 5.88 and 8.88×10^{-12} dyne cm.

Random Number Trajectories. Simulated trajectories in the presence and absence of the force arising from the torsion potential were performed using the same "trajectory" of random numbers for the fluctuating displacements, $f_i(\Delta t)$ and $\mathbf{S}_i(\Delta t)$, $i = 1, \ldots N$, over the successive time intervals Δt. Hence, statistical errors in the simulation make no contribution to any *differences* between such trajectories in the presence and absence of that force.

Analysis of Simulated *r*(*t*) Data. The analytical theory is fitted to the simulated $r(t)$ data by an iterative nonlinear least-squares procedure, which is similar to that employed in our data analysis program. The only adjustable parameter is the torsion constant α, since the initial amplitude is fixed at $r(0) = 0.4$ in this case. The simulated data in each case are fitted over two time spans, namely, 0−50 and 0−100 ns. The best-fit torsion constants for these two time spans are then averaged to obtain the final value. This protocol is similar to that followed in the analysis of experimental anisotropy data.[1]

Results and Discussion

Effects of Forces Arising from the Torsion Potential. A comparison of optical anisotropy ($r(t)$) data that were simulated in the presence and absence of the forces ($(\mathbf{F}_t(t))_j$, $j = 1, \ldots N$) arising from the torsion potential, but with the corresponding torques always present, is displayed in Figure 1. In the case of either linear or circular DNAs, the data from the two simulations agree extremely closely. Evidently, these forces from the torsion potential exert a negligible effect on the orientational dynamics of equilibrium trajectories over the time span examined. In contrast, when the system begins very far from equilibrium, for example, as a planar circle with a nonvanishing linking difference, the initial rate of equilibration of the writhe depends very strongly on the presence of forces arising from the torsion potential. This was demonstrated by Chirico and Langowski[25] and confirmed also in the present work (data not shown). Our results for the evolution of the writhe along such a trajectory closely resemble those in Figure 7 of ref 25. Thus, despite the substantial effect of such forces in the initial writhing of a planar circle with net torsional strain, they have virtually no influence on the optical anisotropy along an equilibrium trajectory. The omission of such forces, then, from the analytical theory is not expected to produce significant errors in the analysis of typical FPA data, which represent equilibrium trajectories.

Test of the Analytical Theory and Data Analysis Protocol on Simulated Data. The analytical theories give rather good fits to the $r(t)$ data from simulations in which all forces are included. Typical comparisons of the best-fit analytical curves with the simulated data for linear and circular DNAs are presented in Figures 2 and 3, respectively. Clearly, the analytical theories with the best-fit torsion constants closely follow the simulated $r(t)$ curves for both species. Average best-fit torsion constants (from the 0−50 and 0−100 ns time spans) are listed in Table 1 along with the ratios, α_{in}/α_{bf}, of the input to average best-fit torsion constants in each case. The important point is that these ratios are fairly close to 1.0. This further demonstrates the good agreement between the analytical theories and the simulations. Such ratios are the correction factors, by which the best-fit torsion constants obtained from the analysis of experimental $r(t)$ data should be corrected in order to obtain the best possible values. Such α values are the best estimates of those that would have

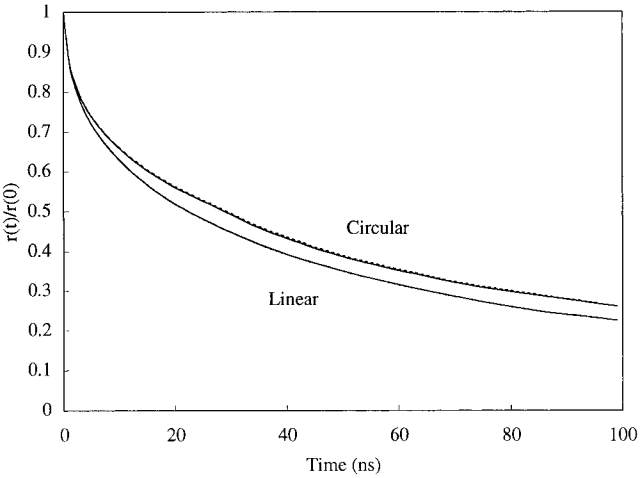

Figure 1. Simulated optical anisotropy $r(t)$ vs time t. The upper pair of curves pertains to circular DNA, and the lower pair pertains to linear DNA. Upper and lower *solid* curves are results of Brownian dynamics simulations that include the force arising from the torsion potential. Upper and lower *dashed* curves, which are partially or entirely obscured by the solid curves, are the results of Brownian dynamics simulations that omit the force arising from the torsion potential. Simulations apply to chains consisting of $N = 21$ subunits of length $b = 31.8$ Å, which corresponds to 196 bp. The torsion constant between subunits, $\alpha_0 = 6.29 \times 10^{-13}$ dyne cm, corresponds to a torsion constant between base pairs, $\alpha = 5.88 \times 10^{-12}$ dyne cm. Other parameters are the dynamic persistence length $P_d = 1500$ Å, subunit (sphere) hydrodynamic radius, $a = 15.9$ Å, subunit translational friction factor, $f = 6\pi\eta a = 3 \times 10^{-8}$ dyne cm^{-1} s, subunit (cylinder) hydrodynamic radius, $r_{cyl} = 12$ Å, and friction factor for azimuthal rotation of a subunit $\gamma = 4\eta b\pi r_{cyl}^2 = 5.75 \times 10^{-22}$ dyne cm s. The temperature is $T = 293$ K, and $\eta = 0.01$ P. The angle between the transition dipole and the helix axis is $\epsilon_0 = 71.5°$. The stretching force constant is $q = 400$ dyne cm^{-1}, and the parameters of the excluded volume potential are $\sigma = 35$ Å and $\epsilon = 1.56 \times 10^{-5}$ cm. The linking difference of the circle is $\Delta l = 0$. For the linear DNA, $D_R = 4.34 \times 10^4$ s^{-1}, and for the circular DNA, $D_R = 2.07 \times 10^5$ s^{-1}.

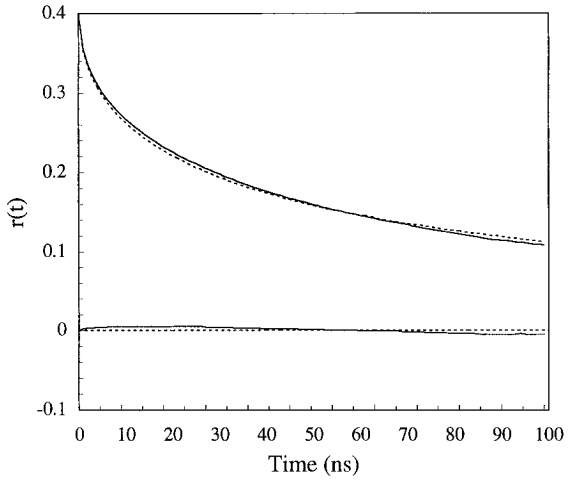

Figure 2. Comparison of simulated and best-fit theoretical values of the optical anisotropy for the linear DNA. (Top) $r(t)$ vs t. The solid curve is the simulated data with $\alpha = 5.88 \times 10^{-12}$ dyne cm, and the dashed curve is the best-fit theoretical model function with $\alpha = 5.14 \times 10^{-12}$ dyne cm. Other parameters are as indicated in the legend of Figure 1. (Bottom) Difference between the simulated and best-fit theoretical curves.

Table 1. Comparison of Average Best-Fit and Input Values of the Torsion Constant α

linear DNAs			circular DNAs		
input α (dyne cm)	best-fit α[a] (dyne cm)	correction factor[b]	input α (dyne cm)	best-fit α[a] (dyne dm)	correction factor[b]
2.00×10^{-12}	1.91×10^{-12}	1.05	2.00×10^{-12}	2.09×10^{-12}	0.957
3.00×10^{-12}	2.82×10^{-12}	1.06	3.00×10^{-12}	3.09×10^{-12}	0.971
4.00×10^{-12}	3.772×10^{-12}	1.08	4.00×10^{-12}	4.07×10^{-12}	0.983
5.00×10^{-12}	4.61×10^{-12}	1.08	5.00×10^{-12}	5.02×10^{-12}	0.996
5.88×10^{-12}	5.38×10^{-12}	1.09	5.88×10^{-12}	5.83×10^{-12}	1.01
			8.82×10^{-12}	8.46×10^{-12}	1.04

[a] Average of best-fit α values obtained by analyzing the simulated data over two time spans, 0−50 and 0−100 ns. [b] Correction factor is the ratio, α_{in}/α_{bf}, of input to average best-fit values.

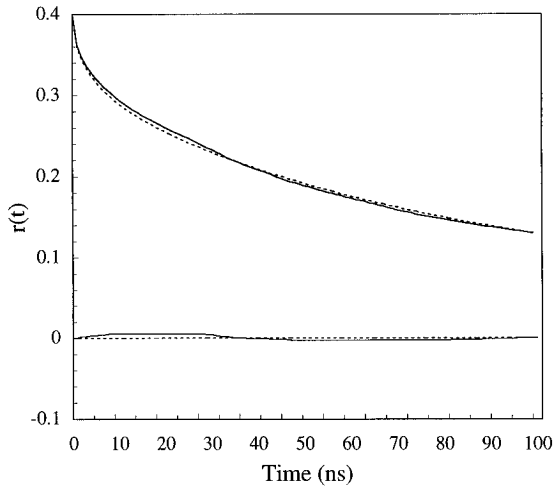

Figure 3. Comparison of simulated and best-fit theoretical values of the optical anisotropy $r(t)$ for a circular 196 bp DNA. (Top) $r(t)$ vs t. The solid curve is the simulated data with $\alpha = 8.82 \times 10^{-12}$ dyne cm, and the dashed curve is the best-fit theoretical model function with $\alpha = 8.20 \times 10^{-12}$ dyne cm. Other parameters are as indicated in legend of Figure 1. (Bottom) Difference between the simulated and best-fit theoretical curves.

been obtained, if the data had been fitted iteratively by Brownian dynamics simulations of very high statistical precision instead of by the less complete analytical theory. The comparatively good agreement in the case of the small circles provides some justification for the approximations made in the analytical treatment of the circular filaments.

This is the first quantitative test of our analytical theory for the simultaneous twisting and bending dynamics of a mode filament against a full Brownian dynamics simulation containing all of the relevant forces. The high quality of the fits and the relatively close proximity of the α_{in}/α_{bf} ratios to 1.0 inspire some confidence that fairly precise torsion constants can be extracted from experimental data for small linear and circular DNAs by fitting the analytical theory to the data, and then scaling the best-fit torsion constant by the appropriate correction factor α_{in}/α_{bf}. Of course, this is all predicated on the presumption that the *dynamic* bending rigidity, or *dynamic* persistence length,[1,41,47] of the DNA is known. In this work, we have employed our current best guess ($P = 1500$ Å) for that quantity,[14] but that issue is by no means completely resolved for either linear or small circular DNAs.

The origin of the small discrepancies between the best-fit and input torsion constants is not known with certainty, but two possibilities should be mentioned. First, the analytical treatment of the bending dynamics is already approximate for the linear DNA, and even more so for the circular species. Second, stretching springs are incorporated into the Brownian dynamics simulations, but not into the analytical theory. Whether either of these differences between the analytical theory and the simulations could account for the observed slight discrepancies between the best-fit and input values of the torsion constant is a matter for future study.

Acknowledgment. This work was supported in parts by an NSF grant (MCB-9817042) to J.M.S. and an NIH grant (GM46516) to S.A.A.

Appendix A. Forces and Torques for the Brownian Dynamics Algorithm

Coordinate Frames. A coordinate frame defined by the *unit* vectors ($\mathbf{f}_i$, $\mathbf{v}_i$, $\mathbf{u}_i$) is fixed in each subunit i, $i = 1, 2, \ldots N$, of the chain. The local z_i-axis, namely, $\mathbf{u}_i = \mathbf{b}_i/|\mathbf{b}_i|$, is chosen to lie along the bond vector ($\mathbf{b}_i$) from the ith to $(i + 1)$th subunit. The local x_i- and y_i-axes are perpendicular to $\mathbf{u}_i$ and to each other and are parallel to $\mathbf{f}_i$ and $\mathbf{v}_i$, respectively. The coordinate frames in successive subunits are chosen so that, when the twisting and bending potential energy of the $j-(j + 1)$ "springs" both vanish, the $\mathbf{f}_{i+1}$, $\mathbf{v}_{i+1}$, $\mathbf{u}_{i+1}$ are parallel to, respectively, the $\mathbf{f}_i$, $\mathbf{v}_i$, $\mathbf{u}_i$. Though not needed in the present treatment, in the event that the bending potential is anisotropic, so the filament bends like a ribbon, $\mathbf{f}_i$ is chosen to lie in the plane of the ribbon, and $\mathbf{v}_i = \mathbf{u}_i \times \mathbf{f}_i$.

Potential Energy. The potential energy of the model filament is assumed to be given by

$$U^{tot} = U_b + U_t + U_s + U_{ex} \tag{A1}$$

wherein the bending potential is given by

$$U_b = (\kappa_\beta/2)\sum_{j=1}^{N}\beta_{j,j+1}^2 \tag{A2}$$

where $\beta_{j,j+1}$ is the angle between $\mathbf{u}_j$ and $\mathbf{u}_{j+1}$. The torsion potential is given by

$$U_t = (g/2)\sum_{j=1}^{N}(\alpha_{j,j+1} + \gamma_{j,j+1} - \phi_0)^2 \tag{A3}$$

$$= (g/2)\sum_{j=1}^{N}(\phi_{j,j+1} - \phi_0)^2 \tag{A4}$$

where $\phi_{j,j+1} \equiv \alpha_{j,j+1} + \gamma_{j,j+1}$ is the net twist from the jth to the $(j + 1)$th subunit, and ϕ_0 is the intrinsic succession angle. The stretching potential is given by

$$U_s = (q/2)\sum_{j=1}^{N}(b_j - b)^2 \tag{A5}$$

where $b_j = |\mathbf{b}_j|$ and b is the intrinsic bond length. The excluded volume potential is given by

$$U_{ex} = (^1/_2)\sum\sum_{i\neq j} V(|\mathbf{r}_i - \mathbf{r}_j|) \tag{A6}$$

$$V(r) = \begin{cases} \epsilon\left[\left(\frac{\sigma}{r}\right)^{12} - \left(\frac{\sigma}{r}\right)^{6}\right], & \text{when } r < \sigma \\ 0, & \text{when } r > \sigma \end{cases} \tag{A7}$$

The quantities κ_β and g are the torque constants for bending and twisting, respectively, and q is the force constant for stretching. In this work the Lennard-Jones diameter is taken to be $\sigma = 35$ Å.

The potential energy depends only upon various relative coordinates of the subunits, in other words, upon the internal configuration of the chain, and is completely independent of the position and overall orientation of that chain in the laboratory frame.

Coordinates. Infinitesimal displacements of the chain from its current position are completely specified by the $4N$ independent infinitesimal coordinates, $\{(\delta\mathbf{r}_i)_c, \delta R_{zi};\ i = 1, \ldots N\}$, wherein δR_{zi} is an infinitesimal rotation of the ith subunit around its own body-fixed z_i-axis, and $(\delta\mathbf{r}_i)_c$ is an infinitesimal translation of the ith subunit *subject to the constraint that none of the subunits are rotated around their own z-axes*. This constraint is *required* to ensure that the $(\delta\mathbf{r}_i)_c$ and δR_{zi} actually vary independently. These coordinates must also be infinitesimal (very small in practice) so that the rotations $\{\delta R_{xi}, \delta R_{yi};\ i = 1, \ldots N\}$ induced by the translations $[(\delta\mathbf{r}_i)_c, i = 1, \ldots N\}$ commute with the $\{\delta R_{zi}, i = 1, \ldots N\}$, in which case the order of making the $\{(\delta\mathbf{r}_i)_c, i = 1, \ldots N\}$ and the $\{R_{zi}, i = 1, \ldots N\}$ displacements has no effect. The Brownian dynamics moves consist alternately of subunit rotations around their own z-axes with absolutely no translations (i.e., $\{\delta R_{zi}, i = 1, \ldots N\}$) followed by translations of the subunits with absolutely no rotations around their own z-axes (i.e., $\{(\delta\mathbf{r}_i)_c, i = 1, \ldots N\}$).

The next problem is to find a set of independent, infinitesimal, *local or internal* coordinates, in terms of which gradients of the potential energy with respect to either a subunit position or a subunit azimuthal orientation around its own z-axis can be expressed, while rigorously enforcing the necessary constraints. In addition, the resulting forces and torques should, for computational convenience, be expressed in terms of the unit vectors $\{\mathbf{f}_i, \mathbf{v}_i, \mathbf{u}_i;\ i = 1, \ldots N\}$ in the laboratory frame, the frame-to-frame Euler angles $\{\alpha_{i,i+1}, \beta_{i,i+1}, \gamma_{i,i+1}\}$, and the bond lengths $\{b_i, i = 1, \ldots N\}$. The standard convention is adopted for the Euler rotation $\Phi_{i,i+1} = (\alpha_{i,i+1}, \beta_{i,i+1}, \gamma_{i,i+1})$ that carries a coordinate frame from coincidence with the ith frame to coincidence with the $(i + 1)$th. Specifically, the rotations are performed in succession, first by $\alpha_{j,j+1}$ around z_j, then by $\beta_{j,j+1}$, around the new y_j'-axis of the rotated frame, and finally by $\gamma_{j,j+1}$ around the still newer z_j''-axis of the rotated frame, which lies along z_{j+1}.

The *force* on the ith bead is calculated as the negative gradient of the potential energy with respect to $(\delta\mathbf{r}_i)_c$, subject to the constraints that (1) all *other* bead positions remained fixed, that is, $\{(\delta\mathbf{r}_j)_c = 0,\ j \neq i\}$, and (2) no rotations of any subunit around its own z-axis take place, that is, $\{\delta R_{zj} = 0,\ j = 1, \ldots N\}$. When the ith subunit is *translated* in such a way that the positions of the other beads remain fixed, it is generally required that the coordinate frames of *both* the $(i - 1)$th and ith subunits *rotate* (in the laboratory frame or in any other stationary frame). In general, $\delta R_{x,i-1}$, $\delta R_{y,i-1}$, δb_{i-1} and also δR_{xi}, δR_{yi}, δb_i vary with $(\delta\mathbf{r}_j)_c$. The three coordinates comprising $(\delta\mathbf{r}_i)_c$ imply, and are implied by, either triplet $(\delta R_{x,i-1}, \delta R_{y,i-1}, \delta b_{i-1})$ or $(\delta R_{xi}, \delta R_{yi}, \delta b_i)$; hence each triplet specifies the other, and only one or the other is actually independent. In computing gradients of any particular term in the potential energy, it is permissible to use either triplet of coordinates, though not both simultaneously. In addition, the appropriate local coordinate for rotation of the ith subunit around its own z-axis is δR_{zi}. Hence, the overall infinitesimal displacement defined by $(\delta\mathbf{r}_i)_c$ plus δR_{zi} can be expressed completely by either $(\delta R_{xi}, \delta R_{yi}, \delta b_i, \delta R_{zi})$ or $(\delta R_{x,i-1}, \delta R_{y,i-1}, \delta b_{i-1}, \delta R_{zi})$. The *local* infinitesimal coordinates within either quartet are completely independent of the other coordinates in the same quartet.

Excluded Volume Forces. Since U_{ex} depends only upon the relative positions of the beads and is independent of any local angular coordinates, its gradient may be evaluated directly to give[25]

$$(\mathbf{F}_{ex})_i = -\frac{\partial U_{ex}}{\partial \mathbf{r}_i} = \sum_{j\neq i} -6(\epsilon/\sigma)(\sigma/r_{ij})^7[1 - 2(\sigma/r_{ij})^6]\hat{\mathbf{r}}_{ij} \tag{A8}$$

where $r_{ij} = |\mathbf{r}_i - \mathbf{r}_j|$ and $\hat{\mathbf{r}}_{ij} = (\mathbf{r}_i - \mathbf{r}_j)/|\mathbf{r}_i - \mathbf{r}_j|$.

Stretching Forces. The displacement $(\delta\mathbf{r}_i)_c$ causes changes in b_{i-1} and b_i, so only the $j = i - 1$ and $j = i$ terms in eq A5 contribute to the force on the ith subunit. The gradient of the $j = i - 1$ term in U_s is calculated via $(\delta b_{i-1}/\partial\mathbf{r}_i)(\partial/\partial b_{i-1})$ while that of the $j = i$ term is calculated via $(\partial b_i/\partial\mathbf{r}_i)(\partial/\partial b_i)$. Hence, each contribution is evaluated using one or the other of the independent local coordinates, b_{i-1} or b_i. Using $\partial b_{i-1}/\partial\mathbf{r}_i = \mathbf{u}_{i-1}$ and $\partial b_i/\partial\mathbf{r}_i = -\mathbf{u}_i$, one obtains[25,32]

$$(\mathbf{F}_s)_i = -q[-(b_i - b)\mathbf{u}_i + (b_{i-1} - b)\mathbf{u}_{i-1}] \tag{A9}$$

Bending Forces. The bending potential U_b depends only upon the angles between the z_j-axes, or $\mathbf{u}_j$ vectors, of successive subunits. The displacement $(\delta\mathbf{r}_i)_c$ causes changes in two of the $\mathbf{u}_j$, namely, $\mathbf{u}_{i-1}$ and $\mathbf{u}_i$, hence also in $\beta_{i-2,i-1}$, $\beta_{i-1,i}$, and $\beta_{i,i+1}$, so only the $j = i - 2$, $i - 1$, and i terms in eq A2 contribute to the force on the ith subunit. The change $\delta\beta_{j-1,j}$ is dependent of either δR_{zj} or $\delta R_{z,j-1}$, as demonstrated explicitly by eq A18 below and extensions thereof, so the constraint that $\{\delta R_{zj} = 0,\ j = 1, \ldots N\}$ is irrelevant for the evaluation of the bending force. Upon making use of the relations

$$\frac{\partial\beta_{j-1,j}}{\partial\mathbf{u}_j} = \frac{(-)\mathbf{u}_{j-1}}{\sin(\beta_{j-1,j})}; \qquad \frac{\partial\beta_{j-1,j}}{\partial\mathbf{u}_{j-1}} = \frac{(-)\mathbf{u}_j}{\sin(\beta_{j-1,j})} \tag{A10}$$

and[25,32]

$$\frac{\partial\mathbf{u}_{i-1}}{\partial\mathbf{r}_i} = (\mathbf{l} - \mathbf{u}_{i-1}\mathbf{u}_{i-1})/b_{i-1}; \qquad \frac{\partial\mathbf{u}_i}{\partial\mathbf{r}_i} = -(\mathbf{l} - \mathbf{u}_i\mathbf{u}_i)/b_i \tag{A11}$$

one obtains[25]

$$(\mathbf{F}_b)_i = -\kappa_\beta \sum_{j=i-1}^{i+1} \beta_{j-1,j}\left(\frac{\partial\beta_{j-1,j}}{\partial\mathbf{u}_{j-1}}\cdot\frac{\partial\mathbf{u}_{j-1}}{\partial\mathbf{r}_i} + \frac{\partial\beta_{j-1,j}}{\partial\mathbf{u}_j}\cdot\frac{\partial\mathbf{u}_j}{\partial\mathbf{r}_i}\right)$$
$$= -\kappa_\beta[+\mathbf{A}_i - \mathbf{A}_{i-1} + \mathbf{B}_i - \mathbf{B}_{i-1}] \quad \text{(A12)}$$

where

$$\mathbf{A}_j = \beta_{j,j+1}(\mathbf{u}_{j+1} - \mathbf{u}_j\cos(\beta_{j,j+1}))/b_j\sin(\beta_{j,j+1})$$
$$= \beta_{j,j+1}(\mathbf{f}_j\cos(\alpha_{j,j+1}) + \mathbf{v}_j\sin(\alpha_{j,j+1}))/b_j \quad \text{(A13)}$$

and

$$\mathbf{B}_j = \beta_{j-1,j}(\mathbf{u}_{j-1} - \mathbf{u}_j\cos(\beta_{j-1,j}))/b_j\sin(\beta_{j-1,j})$$
$$= \beta_{j-1,j}(-\mathbf{f}_j\cos(\gamma_{j-1,j}) + \mathbf{v}_j\sin(\gamma_{j-1,j}))/b_j \quad \text{(A14)}$$

The first forms given for $\mathbf{A}_j$ and $\mathbf{B}_j$ in eqs A13 and A14 are the most convenient for simulating wormlike chains in the *absence* of the force arising from the torsion potential, since it is not required to evaluate the $\alpha_{j,j+1}$ and $\gamma_{j,j+1}$ Euler angles in that case. However, since it is necessary to evaluate the $\alpha_{j,j+1}$ and $\gamma_{j,j+1}$ Euler angles in order to calculate the forces arising from the torsion potential, the second forms given for $\mathbf{A}_j$ and $\mathbf{B}_j$ may be more convenient in that case, since division by $\sin\beta_{j,j+1}$, which may vanish, is not required for evaluation of those expressions.

Forces Arising from the Torsion Potential. In this derivation, we explicitly enforce the constraint $\{\delta R_{zj} = 0, j = 1, \ldots N\}$, while calculating the gradient of the torsion potential U_t. First, we note that

$$(\mathbf{F}_t)_i = -g\{P_{i-2,i-1}(\partial(\alpha_{i-2,i-1} + \gamma_{i-2,i-1})/\partial\mathbf{r}_i)_c +$$
$$P_{i-1,i}(\partial(\alpha_{i-1,i} + \gamma_{i-1,i})/\partial\mathbf{r}_i)_c +$$
$$P_{i,i+1}(\partial(\alpha_{i,i+1} + \gamma_{i,i+1})/\partial\mathbf{r}_i)_c\} \quad \text{(A15)}$$

wherein

$$P_{j,j+1} = (\alpha_{j,j+1} + \gamma_{j,j+1} - \phi_0) \quad \text{(A16)}$$

is the local twisting strain, and the subscript c denotes the constraint. The constraints in eq A15 can be enforced by first expressing the $\delta(\alpha_{j,j+1} + \gamma_{j,j+1})$ in terms of the independent coordinate frame rotations, $\delta R_{x,i-1}$, $\delta R_{y,i-1}$ or δR_{xi}, δR_{yi}, in the following way.

The rotations of the $(i-1)$th and ith beads, due to the translation $(\delta\mathbf{r}_i)_c$, cause variations in three frame-to-frame Euler rotations, $\delta\Phi_{i-2,i-1}$, $\delta\Phi_{i-1,i}$, and $\delta\Phi_{i,i+1}$, which can be simply expressed in terms of the coordinate frame rotations, $\delta R_{x,i-1}$, $\delta R_{y,i-1}$ or δR_{xi}, δR_{yi}. We first consider rotating the jth subunit while holding the $(j-1)$th fixed. For this case, the canonical small-angle relations[38] give

$$\delta\alpha_{j-1,j} = \frac{-\cos(\gamma_{j-1,j})}{\sin(\beta_{j-1,j})}\delta R_{xj} + \frac{\sin(\gamma_{j-1,j})}{\sin(\beta_{j-1,j})}\delta R_{yj} \quad \text{(A17)}$$

$$\delta\beta_{j-1,j} = \sin(\gamma_{j-1,j})\,\delta R_{xj} + \cos(\gamma_{j-1,j})\,\delta R_{yj} \quad \text{(A18)}$$

$$\delta\gamma_{j-1,j} = \frac{\cos(\gamma_{j-1,j})\cos(\beta_{j-1,j})}{\sin(\beta_{j-1,j})}\delta R_{xj} -$$
$$\frac{\sin(\gamma_{j-1,j})\cos(\beta_{j-1,j})}{\sin(\beta_{j-1,j})}\delta R_{yj} + \delta R_{zj} \quad \text{(A19)}$$

It is required to set $\delta R_{zj} = 0$ in the third equation, whenever the rotation arises as a consequence of $(\delta\mathbf{r}_j)_c$.

Next we consider rotating the jth subunit while holding the $(j+1)$th fixed. Then $\delta\Phi_{j+1,j}$ is obtained by moving backward along the chain from the $(j+1)$th to the jth subunit. One first obtains $\delta\Phi_{j+1,j} = (\delta\alpha_{j+1,j}, \delta\beta_{j+1,j}, \delta\gamma_{j+1,j})$ by setting $j = j$ and $j - 1 = j + 1$ in eqs 17−A19. Then $\delta\Phi_{j,j+1}$ is determined from $\delta\Phi_{j+1,j}$ according to the relation $\delta\Phi_{j,j+1} = (\delta\alpha_{j,j+1}, \delta\beta_{j,j+1}, \delta\gamma_{j,j+1}) = \delta\Phi_{j+1,j}^{-1} = (-\delta\gamma_{j+1,j}, -\delta\beta_{j+1,j}, -\delta\alpha_{j+1,j})$. This yields finally

$$\delta\alpha_{j,j+1} = \frac{\cos(\alpha_{j,j+1})\cos(\beta_{j,j+1})}{\sin\beta_{j,j+1}}\delta R_{xj} +$$
$$\frac{\sin(\alpha_{j,j+1})\cos(\beta_{j,j+1})}{\sin\beta_{j,j+1}}\delta R_{yj} - \delta R_{zj} \quad \text{(A20)}$$

$$\delta\beta_{j,j+1} = \sin(\alpha_{j,j+1})\,\delta R_{xj} - \cos(\alpha_{j,j+1})\,\delta R_{yj} \quad \text{(A21)}$$

$$\delta\gamma_{j,j+1} = \frac{-\cos(\alpha_{j,j+1})}{\sin(\beta_{j,j+1})}\delta R_{xj} - \frac{\sin(\alpha_{j,j+1})}{\sin(\beta_{j,j+1})}\delta R_{yj} \quad \text{(A22)}$$

Now, $\delta\Phi_{i-2,i-1}$ is obtained from eqs A17−A19 by setting $j = i - 1$ and $j - 1 = i - 2$, and $\delta\Phi_{i,i+1}$ is obtained from eqs A20−A22 by setting $j = i$ and $j + 1 = i + 1$. Finally, $\delta\Phi_{i-1,i}$ is obtained as the sum of two contributions, namely, (1) the case when the ith subunit rotates while the $(i-1)$th is held fixed, and (2) the case when the $(i-1)$th bead rotates while the ith remains fixed. The first contribution (1) is obtained from eqs A17−A19 by setting $j = i$ and $j - 1 = i - 1$, while the second contribution (2) is obtained from eqs A20−A22 by setting $j = i - 1$, $j + 1 = i$. In this way, each contribution to $\delta\Phi_{i-2,i-1}$, $\delta\Phi_{i-1,i}$, and $\delta\Phi_{i,i+1}$ is expressed exclusively in terms of one or the other set of independent infinitesimal local coordinates, namely, δR_{xi}, δR_{yi} or $\delta R_{x,i-1}$, $\delta R_{y,i-1}$. After summing the appropriate pairs of contributions, one obtains (with $\{\delta R_{zj} = 0, j = 1, \ldots N\}$):

$$\delta(\alpha_{i-2,i-1} + \gamma_{i-2,i-1}) =$$
$$\frac{(1 - \cos(\beta_{i-2,i-1}))}{\sin(\beta_{i-2,i-1})}(-\cos(\gamma_{i-2,i-1})\,\delta R_{x,i-1} +$$
$$\sin(\gamma_{i-2,i-1})\,\delta R_{y,i-1}) \quad \text{(A23)}$$

$$\delta(\alpha_{i,i+1} + \gamma_{i,i+1}) =$$
$$\frac{(1 - \cos(\beta_{i,i+1}))}{\sin(\beta_{i,i+1})}(-\cos(\alpha_{i,i+1})\,\delta R_{xi} - \sin(\alpha_{i,i+1})\,\delta R_{yi}) \quad \text{(A24)}$$

$$\delta(\alpha_{i-1,i} + \gamma_{i-1,i}) =$$
$$\frac{(1 - \cos(\beta_{i-1,i}))}{\sin(\beta_{i-1,i})}(-\cos(\gamma_{i-1,i})\,\delta R_{xi} + \sin(\gamma_{i-1,i})\,\delta R_{yi} -$$
$$\cos(\alpha_{i-1,i})\,\delta R_{x,i-1} - \sin(\alpha_{i-1,i})\,\delta R_{y,i-1}) \quad \text{(A25)}$$

In order to evaluate the gradients $(\partial(\alpha_{j,j+1} + \gamma_{j,j+1})/\delta\mathbf{r}_i)_c$ from eqs A23−A25, it is first necessary to make use of the relation between the changes in the unit vectors, $\delta\mathbf{f}_j$, $\delta\mathbf{v}_j$, $\delta\mathbf{u}_j$, and δR_{xj}, δR_{yj} (holding $\delta R_{zj} = 0$). In general, for small rotations,

$$\delta\mathbf{f}_j = -\delta R_{yj}\,\mathbf{u}_j + \delta R_{zj}\,\mathbf{v}_j \quad \text{(A26)}$$

$$\delta\mathbf{v}_j = -\delta R_{zj}\,\mathbf{f}_j + \delta R_{xj}\,\mathbf{u}_j \quad \text{(A27)}$$

$$\delta\mathbf{u}_j = -\delta R_{xj}\,\mathbf{v}_j + \delta R_{yj}\,\mathbf{f}_j \quad \text{(A28)}$$

Equation A28 yields

$$(\partial R_{xi}/\partial \mathbf{r}_i) = -\mathbf{v}_i\cdot(\partial \mathbf{u}_i/\partial \mathbf{r}_i) \quad \text{(A29)}$$

$$(\partial R_{x,i-1}/\partial \mathbf{r}_i) = -\mathbf{v}_{i-1}\cdot(\partial \mathbf{u}_{i-1}/\partial \mathbf{r}_i) \quad \text{(A30)}$$

$$(\partial R_{yi}/\partial \mathbf{r}_i) = \mathbf{f}_i\cdot(\partial \mathbf{u}_i/\partial \mathbf{r}_i) \quad \text{(A31)}$$

$$(\partial R_{y,i-1}/\partial \mathbf{r}_i) = \mathbf{f}_{i-1}\cdot(\partial \mathbf{u}_{i-1}/\partial \mathbf{r}_i) \quad \text{(A32)}$$

The gradients $\partial \mathbf{u}_i/\partial \mathbf{r}_i$ and $\partial \mathbf{u}_{i-1}/\partial \mathbf{r}_i$ are given by eqs A11. Now, after making use of eqs A29−A32, A11, and the relation, $(1 - \cos(\beta_{i-1,i}))/\sin(\beta_{i-1,i}) = \tan(\beta_{i-1,i}/2)$, in eqs A23−A25, which are in turn substituted into eq A15, and collecting terms, one obtains

$$(\mathbf{F}_t)_i = g(\chi_i - \chi_{i-1}) \quad \text{(A33)}$$

wherein

$$\chi_i = P_{i,i+1}\frac{\tan(\beta_{i,i+1}/2)}{b_i}[\cos(\alpha_{i,i+1})\,\mathbf{v}_i - \sin(\alpha_{i,i+1})\mathbf{f}_i] + P_{i-1,i}\frac{\tan(\beta_{i-1,i}/2)}{b_i}[\cos(\gamma_{i-1,i})\,\mathbf{v}_i + \sin(\gamma_{i-1,i})\mathbf{f}_i] \quad \text{(A34)}$$

Equations A33 and A34 for the force arising from the torsion potential can be proved to be completely equivalent to the result of Chirico and Langowski.[25] However, the present formulas are considerably simpler and computationally more convenient, since there are no potentially vanishing denominators with which to contend.

The present derivation of $(\mathbf{F}_t)_i$ appears to be rigorously correct. It improves on the treatment of Chirico and Langowski in three main respects. First, the question of which variables constitute a proper set of *independent* coordinates is clarified substantially. As shown by Chirico and Langowski, the subunit z-axis rotations $\{\delta R_{zj}, j = 1, \ldots N\}$ are neither necessarily nor automatically independent of the subunit translations $\{\delta \mathbf{r}_j, j = 1, \ldots N\}$. Consequently, the independence of such coordinates was assumed in that work. In fact, the infinitesimal subunit z-axis rotations $\{\delta \mathbf{R}_{zj}, j = 1, \ldots N\}$ are independent of the subunit translations $\{(\delta \mathbf{r}_j)_c; j = 1, \ldots N\}$ *only* when the rotations of the coordinate frames in response to such translations are carried out in such a way that $\{\delta R_{zj} = 0, j = 1, \ldots N\}$. Despite the absence of any subunit z-axis rotations during the infinitesimal subunit translations, the resulting change in writhe must be compensated by a change of opposite sign in the total twist, $t = \sum_{i=1}^{N}(\alpha_{i,i+1} + \gamma_{i,i+1})$. This demonstrates clearly that the frame-to-frame twists, $\phi_{i,i+1} = \alpha_{i,i+1} + \gamma_{i,i+1}$, necessarily change as a consequence of subunit translations, even when the subunits themselves do not rotate around their own z-axes. Second, the constraints $\{\delta R_{zj} = 0, j = 1, \ldots N\}$ are *explicitly* enforced from the outset, when calculating the gradient of U_t with respect to $(\delta \mathbf{r}_i)_c$. In contrast, Chirico and Langowski *implicitly* enforced the same constraint of no z-axis subunit rotations by applying the last two of their eqs 4 in the final step of their gradient calculation, so they obtained the same (correct) result, albeit in a somewhat different form. Though intuitively reasonable, it was not entirely clear whether those constraints applied as well to all other steps in gradient calculation, or only to the final step. The present treatment proves the validity of the procedure adopted by Chirico and Langowski. Third, the expression in eq A34 is considerably simpler than that of Chirico and Langowski[25] and more convenient for numerical computation since it contains no potentially vanishing factors in the denominator.

It is apparent from eqs A33 and A34 that the forces arising from the torsion potential all vanish for straight chains, for which the bending angles all vanish $\{\beta_{i,i+1} = 0, i = 1, \ldots N\}$, regardless of the local torsional strains $\{\alpha_{i,i+1} + \gamma_{i,i+1} - \phi_0; i = 1, \ldots N\}$. They also vanish, whenever the local torsional strains all vanish, regardless of the local bending angles. In fact, this force causes bent segments to writhe in the presence of uniform torsional strains, and to undergo crankshaft motions in the presence of nonuniform torsional strains.

Torques Arising from the Torsion Potential. The torque on the ith subunit is calculated by taking the gradient of the torsion potential with respect to δR_{zi} while holding $(\delta R_{xj} = 0 = \delta R_{yj} = \delta b_j; j = 1, \ldots N)$:

$$(T_t)_i = -g\,(P_{i-1,i}(\partial(\alpha_{i-1,i} + \gamma_{i-1,i})/\partial R_{zi})_d + P_{i,i+1}(\partial(\alpha_{i,i+1} + \gamma_{i,i+1})/\partial R_{zi})_d) \quad \text{(A35)}$$

where the subscript d denotes the constraint $(\delta R_{xj} = 0 = \delta R_{yj} = \delta b_j)$ and the $P_{j,j+1}$ are given by eq A9. Use of eqs A17 and A19 in the first term and eqs A20 and A22 in the second term yields simply

$$(T_t)_i = -g(\alpha_{i-1,i} + \gamma_{i-1,i} - (\alpha_{i,i+1} + \gamma_{i,i+1})) = g(\phi_{i,i+1} - \phi_{i-1,i}) \quad \text{(A36)}$$

in agreement with previous works.[1,28,39]

Appendix B. Normal Mode Theory for the Bending Dynamics of Weakly Bending Circular Chains

A normal mode theory developed previously for the bending dynamics of linear chains[41] is here extended to encompass circular molecules. The model filament consists of N identical spherical beads, whose centers are connected by N bond vectors of fixed length b that sum to zero. The beads are labeled by the index, j, $j = 1, \ldots N$, and the bond vector $\mathbf{b}_j$ extends from the jth to $(j + 1)$th bead. Between each pair of successive beads is a Hookean bending spring that acts to straighten the chain. A coordinate frame is fixed in the molecule in the following way. First, we note that the instantaneous shape of the ring is defined by the instantaneous configuration of the array of bond vectors, which may be regarded as a slightly deformed polygon. We then imagine that a perfect planar polygon with the same number of bond vectors (chords) of the same length (b) is least-squares fitted to the actual configuration of bond vectors. This best-fit perfect planar polygon is the reference configuration. Each bond vector of the reference polygon subtends an angle $\theta_0 = 2\pi/N$ and corresponds to a particular bond vector of the actual deformed polygon. The origin is taken at the center of the reference polygon. The molecular z-axis is taken along the $j = 1$ bond vector of the reference polygon, while the molecular x-axis is taken to be the inwardly directed normal to that bond vector in the plane of the reference polygon. The molecular y-axis is taken normal to the plane of the reference polygon, such that $\hat{\mathbf{x}}$, $\hat{\mathbf{y}}$, $\hat{\mathbf{z}}$ form a right-handed coordinate system. Each bead is assumed to undergo motions in the y-direction normal to the plane of the reference polygon, as well as motions along the radial line defined by the center of the reference polygon and the particular vertex corresponding to the bead in question. That radial line has unit vector $\hat{\mathbf{r}}_j =$

$(-)\cos((j - 3/2)\theta_0)\hat{\mathbf{x}} + \sin((j - 3/2)\theta_0)\hat{\mathbf{z}}$. Changes in the interbead distances as a consequence of these out-of-plane y-motions and in-plane radial motions are ignored. In addition to the two deformational motions just described, each bead may also undergo an in-plane motion perpendicular to its radius, but all beads must undergo such a motion simultaneously with the same sign and amplitude, so as not to extend or contract the filament. This corresponds to uniform rigid-body rotation of the circular filament around its symmetry axis and is treated separately. It is worthwhile to catalogue the uniform rigid-body motions for further reference. Besides uniform rotation around the symmetry axis, there will also be uniform in-plane translations in the $\hat{\mathbf{x}}$ and $\hat{\mathbf{z}}$ directions. In addition, there will be uniform out-of-plane translation in the $\hat{\mathbf{y}}$ direction, as well as rotations around the in-plane axes, $\hat{\mathbf{x}}$ and $\hat{\mathbf{z}}$, which displace subunits out-of-plane in the $\hat{\mathbf{y}}$ direction.

The bending potential energy is given by

$$U_b = (\kappa_\beta/2)\sum_{j=1}^{N}\beta_{j,j+1}^2 \tag{B1}$$

where $\beta_{j,j+1} = \arccos(\hat{\mathbf{u}}_j \cdot \hat{\mathbf{u}}_{j+1})$ and $\hat{\mathbf{u}}_j = \hat{\mathbf{b}}_j/b$ is a unit vector along the jth bond vector. The first objective is to express the potential energy in terms of the small bead displacements that are involved in deformations of the ring. Each actual bond vector has projections on $\hat{\mathbf{x}}$, $\hat{\mathbf{y}}$, and $\hat{\mathbf{z}}$, and these are derived in the following way. First, we consider the projection of the nth actual bond vector onto the xz, or reference, plane. The angles of all vectors in the reference plane are measured with respect to $\hat{\mathbf{z}}$, which is parallel to the $j = 1$ vector of the reference polygon. Let ξ_n denote the angle between the projection of the nth actual bond vector (onto the reference plane) and the nth bond vector of the reference polygon. When there are no deformations in the xz plane, then $\xi_n = 0$ for all n. With this definition of ξ_n, the angle σ_n between the projection of the nth bond vector (onto the reference plane) and $\hat{\mathbf{z}}$ is

$$\sigma_n = \xi_n + (n - 1)\theta_0 \tag{B2}$$

We now define:

$$\Delta_n = \sigma_{n+1} - \sigma_n = \xi_{n+1} - \xi_n + \theta_0 \tag{B3}$$

which is the angle between the projections of the nth and $(n + 1)$th bond vectors onto the plane. For small out-of-plane deformations, the projection of the nth actual bond vector onto the plane is $N_n b((\sin\sigma_n)\hat{\mathbf{x}} + (\cos\sigma_n)\hat{\mathbf{z}})$, and the unit vector $\mathbf{u}_n$ along the actual bond vector is given by

$$\mathbf{u}_n = N_n((b\sin\sigma_n)\hat{\mathbf{x}} + (y_{n+1} - y_n)\hat{\mathbf{y}} + (b\cos\sigma_n)\hat{\mathbf{z}}) \tag{B4}$$

where N_n is the normalization factor. Keeping just the lowest order correction term, one has

$$N_n = (b^2 + (y_{n+1} - y_n)^2)^{-1/2} \cong (1/b)[1 - (1/2)((y_{n+1} - y_n)/b)^2] \tag{B5}$$

Now, we note that to the same order,

$$\begin{aligned}\cos\beta_{n-1,n} &= \mathbf{u}_{n-1}\cdot\mathbf{u}_n \\ &= [\sin\sigma_n \sin\sigma_{n-1} + \cos\sigma_n \cos\sigma_{n-1}] \times \\ &\quad [1 - (1/2)((y_{n+1} - y_n)/b)^2 - \\ &\quad (1/2)((y_n - y_{n-1})/b)^2] + \\ &\quad (y_{n+1} - y_n)(y_n - y_{n-1})/b^2\end{aligned} \tag{B6}$$

Upon making use of the trigonometric identities,

$$\sin\sigma_{n-1} = \sin(\sigma_n - \Delta_{n-1}) = \sin\sigma_n\cos(-\Delta_{n-1}) + \cos\sigma_n\sin(-\Delta_{n-1}) \tag{B7}$$

$$\cos\sigma_{n-1} = \cos(\sigma_n - \Delta_{n-1}) = \cos\sigma_n\cos(-\Delta_{n-1}) - \sin\sigma_n\sin(-\Delta_{n-1}) \tag{B8}$$

there results

$$\begin{aligned}\cos\beta_{n-1,n} &= \cos(-\Delta_{n-1}) \times \\ &\quad [1 - (1/2b^2)((y_{n+1} - y_n)^2 + (y_n - y_{n-1})^2)] + \\ &\quad (1/b^2)(y_{n+1} - y_n)(y_n - y_{n-1})\end{aligned} \tag{B9}$$

Provided the in-plane and out-of-plane displacements are sufficiently small, $\cos\beta_{n-1,n} \cong 1 - (1/2)\beta_{n-1,n}^2$ and $\cos(-\Delta_{n-1}) \cong 1 - (1/2)\Delta_{n-1}^2$, so one obtains finally

$$\begin{aligned}\beta_{n-1,n}^2 &= \Delta_{n-1}^2 + (1/b^2)(y_{n+1}^2 + 4y_n^2 + y_{n-1}^2 - \\ &\quad 4y_{n+1}y_n - 4y_{n-1}y_n + 2y_{n-1}y_{n+1})\end{aligned} \tag{B10}$$

Upon making use of eq B3 and summing over n, one obtains after some rearrangement of terms in the sum:

$$\begin{aligned}\sum_{n=1}^{N}\beta_{n-1,n}^2 &= N\theta_0^2 + \sum_{n=1}^{N}(\xi_{n+1} - \xi_n)^2 + (1/b^2) \times \\ &\quad \sum_{n=1}^{N}(6y_n^2 - 4y_ny_{n-1} - 4y_ny_{n+1} + y_ny_{n-2} + y_ny_{n+2})\end{aligned} \tag{B11}$$

If the radial displacement r_n of each bead is measured from its corresponding vertex in the perfect planar polygon, with positive displacements taken inward, then the angle between the projection of the actual bond vector on the xz plane and the corresponding bond vector of the reference configuration is

$$\xi_n = (r_{n+1}\cos(\theta_0/2) - r_n\cos(\theta_0/2))/b \tag{B12}$$

$$\xi \cong (r_{n+1} - r_n)/b$$

to the lowest order. Then

$$(\xi_{n+1} - \xi_n)^2 = (r_{n+1}^2 + 4r_n^2 + r_{n-1}^2 + 2r_{n-1}r_{n+1} - 4r_nr_{n-1} - 4r_nr_{n+1})/b^2 \tag{B13}$$

and after some rearrangement of terms,

$$\sum_{n=1}^{N}(\xi_{n+1} - \xi_n)^2 = (1/b^2)\sum_{n=1}^{N}(6r_n^2 - 4r_nr_{n-1} - 4r_nr_{n+1} + r_nr_{n-2} + r_nr_{n+2}) \tag{B14}$$

Finally, by using eqs B11 and B14, the bending potential energy can be written as

$$U_b = (\kappa_\beta/2)(N\theta_0^2 + \mathbf{y}^T\,\mathbf{D}\,\mathbf{y} + \mathbf{r}^T\,\mathbf{D}\,\mathbf{r}) \tag{B15}$$

wherein the $N \times N$ martrix $\mathbf{D}$ is now given by

$$\mathbf{D} = \begin{vmatrix} 6 & -4 & 1 & 0 & 0 & 0 & \dots & \dots & 1 & -4 \\ -4 & 6 & -4 & 1 & 0 & 0 & \dots & \dots & 0 & 1 \\ 1 & -4 & 6 & -4 & 1 & 0 & \dots & \dots & 0 & 0 \\ 0 & 1 & -4 & 6 & -4 & 1 & \dots & \dots & 0 & 0 \\ 0 & 0 & \dots & \dots & \dots & 1 & -4 & 6 & -4 & 1 \\ 1 & 0 & \dots & \dots & \dots & 0 & 1 & -4 & 6 & -4 \\ -4 & 1 & \dots & \dots & \dots & 0 & 0 & 1 & -4 & 6 \end{vmatrix} \quad \text{(B16)}$$

which is just the circulant form of the corresponding matrix for the linear chain,[41] and $\mathbf{y}$ denotes an $N \times 1$ vector with elements (y_1, y_2, ... y_N) and $\mathbf{r}$ denotes an $N \times 1$ vector with elements (r_1, r_2, ... r_N). The first term on the rhs of eq 15 is just the minimum bending energy required to circularize the chain. The second two terms are analogous to those for transverse displacements of a linear chain.

Following the previous development, the $N \times 1$ vector of y-forces on the beads is found to be

$$\mathbf{F}_y = -(\kappa_\beta/b^2)\,\mathbf{D}\,\mathbf{y} \quad \text{(B17)}$$

where $\mathbf{F}_y = (F_{y1}, F_{y2}, \dots F_{yN})$, and the Langevin equation for motion of the beads in the y-direction becomes[41]

$$m\ddot{\mathbf{y}} + f\dot{\mathbf{y}} + (\kappa_\beta/b^2)\,\mathbf{HD}\,\mathbf{y} = \mathbf{E}_y(t) \quad \text{(B18)}$$

where $\mathbf{H} = \mathbf{1} + \mathbf{T}_{yy}$ is the $N \times N$ hydrodynamic interaction matrix, and $\mathbf{E}_y(t)$ is the $N \times 1$ vector of fluctuating Brownian forces in the y-direction on the respective beads, m is the bead mass, $f = 6\pi\eta(b/2) = (1/k_BT)\int_0^\infty d\tau\ \langle E_{yj}(0)\ E_{yj}(\tau)\rangle$ is the friction factor on a single bead, and η is the solvent viscosity. Hydrodynamic interactions are incorporated using the tensor of Rotne and Prager[33] and Yamakawa,[34] which gives (for $l \neq m$):

$$\mathbf{T}_{lm} = \frac{3a}{4R_{lm}}\left\{\mathbf{1} + \hat{\mathbf{R}}_{lm}\hat{\mathbf{R}}_{lm} + \frac{2a^2}{R_{lm}^2}\left(\frac{\mathbf{1}}{3} - \hat{\mathbf{R}}_{lm}\hat{\mathbf{R}}_{lm}\right)\right\} \quad \text{(B19)}$$

where $a = b/2$ is the bead radius, and $\hat{\mathbf{R}}_{lm} = (\mathbf{r}_l - \mathbf{r}_m)/|\mathbf{r}_l - \mathbf{r}_m|$ is the unit vector from the lth to the mth bead. For the purpose of calculating hydrodynamic interaction matrix elements, the bead positions are preset at the corresponding vertices of the perfect planar polygon; hence $R_{lm} = 2R_c \sin(\theta_0|l - m|/2) = 2a \sin(\pi|l - m|/N)/\sin(\pi/N)$, wherein $R_c = a/\sin(\theta_0/2) = a/\sin(\pi/N)$ is the radius of the circle that just circumscribes the polygon. For the y-motions, the hydrodynamic interaction matrix elements become

$$H_{lm} = \delta_{lm} + (1 - \delta_{lm})\left(\frac{3}{8}\frac{\sin(\pi/N)}{\sin(\pi|l - m|/N)}\right)\left(1 + \frac{1}{6}\frac{\sin^2(\pi/N)}{\sin^2(\pi|l - m|/N)}\right) \quad \text{(B20)}$$

In this work we do not explicitly treat the r-motions. Instead, we assume that those in-plane bending deformations yield mean-squared angular displacements of the bond vectors in the reference plane that are identical to the out-of-plane mean-squared angular displacements caused by deformations in the y-direction. This assumption is partially justified by the fact that the same force constant matrix $\mathbf{D}$ applies to both motions and by the fact that the hydrodynamic interactions are also very similar for closely neighboring beads, where such interactions are strongest. However, the hydrodynamic interactions of the two motions differ substantially for beads on opposite sides of the ring. Treatment of the r-motions would be rather approximate in any case, due to the nonparallel nature of those radial motions. Although such nonparallel motion does not affect the bending potential to first order in θ_0, it does cause local extension or contraction of the contour to first order in the r-displacements. In contrast, the y-motions extend or contract the contour only to second-order in the y-displacements. Thus, if longitudinal stretching/compression springs were included in this normal mode theory, small r-displacements would be more strongly resisted than small y-displacements. In this normal mode theory, no account is taken of forces on the beads that arise either from contour stretching or from the torsion potential (as derived in Appendix A). Because the entire normal mode theory for circular molecules is approximate in that sense, and because its primary purpose is to provide a sufficiently simple result to use in iterative data fitting, we elected to avoid the complications inherent in any accurate treatment of the r-motion simply by assuming that both r- and y-deformational motions yield the same mean-squared angular displacements of the bond vectors at all times.

The **HD** dynamical matrix in eq B18 is constructed using eqs B16 and B20 and diagonalized by similarity transformation, as described previously in the case of the linear chain. A significant new feature in the case of the circular chain is that **HD** (or **D** alone) has only one zero eigenvalue, corresponding to uniform translation in the y-direction. In the case of the linear chain a second zero eigenvalue, corresponding to a shear, or nascent rotational, motion was encountered, but that is absent in the case of the circle. In fact, there should be two rigid-body rotations of the ring around orthogonal axes that lie in the reference plane. The out-of-plane mean-squared angular displacements of the bond vectors due to those uniform rotations will be simply superimposed in this theory at a later stage. The point is that in reality there are three out-of-plane uniform rigid-body motions, namely, one translation and two rotations. Likewise, there are three-in-plane rigid-body motions, namely, two translations along orthogonal in-plane axes and rotation around the symmetry axis of the circle. As none of the translations contribute to bond vector reorientations, those will be ignored. The in-plane mean-squared angular displacements of the bond vectors due to rotation around the symmetry axis will also be superposed at a later stage. Thus in the case of the circle, only the nonzero eigenvalues and eigenvectors of the **HD** matrix, which correspond to the bending deformations, are actually used together with the contributions of the superposed uniform rotations to evaluate the relevant mean-squared angular displacements of the bond vectors.

Contributions of the out-of-plane bending normal modes to the mean-squared angular displacements of a given bond vector are computed in the same manner as done previously for linear chains. Since all subunits are completely equivalent, it suffices to do this for the $\mathbf{b}_1$ bond vector. The mean-squared angular displacement of that bond vector around its transverse in-plane axis, which corresponds to the molecular x-axis, is given by[41]

$$\langle\Delta_{x1}(t)^2\rangle = 2D_\perp t + 2(b/P)\sum_{l=2}^{N}(S_{2l} - S_{1l})^2(1 - e^{-t/T_l}) \quad \text{(B21)}$$

wherein P is the dynamic persistence length, $1/T_l = \kappa_\beta\Lambda_l/$

b^2f is the decay rate of the lth normal mode, f is the subunit friction factor, Λ_l is the lth eigenvalue of the **HD** matrix, and S_{jl} is the element of the matrix **S** that diagonalizes **HD** by similarity transformation:

$$(\mathbf{S}^{-1}\,\mathbf{HD}\,\mathbf{S})_{lm} = \Lambda_{ll}\delta_{lm} \tag{B22}$$

S_{jl} is the projection of the lth normal mode onto the jth subunit. The eigenvalues Λ_l and right eigenvector elements S_{jl}, $j = 1, \ldots N$, are determined in precisely the same manner as done for the linear chain.[41] The diffusion coefficient, $D_\perp$, for uniform rotation around the in-plane z-axis is calculated for the perfect planar polygon by using the results of Yamakawa and Yamaki.[46] The mean-squared angular displacement of the $\mathbf{b}_1$ bond vector around its transverse out-of-plane axis, which coincides with the molecular y-axis, is similarly given by

$$\langle \Delta_{y1}(t)^2 \rangle = 2D_{||}t + 2(b/P)\sum_{l=2}^{N}(S_{2l} - S_{1l})^2(1 - \mathrm{e}^{-t/T_l}) \tag{B23}$$

where $D_{||}$ is the diffusion coefficient for uniform rotation of the circular filament around its symmetry axis ($\hat{y}$). $D_{||}$ is also calculated for the perfect planar polygon using the results of Yamakawa and Yamaki.[46]

In the event that $D_\perp \cong D_{||}$, which is the case for our small circular filament, one has $\langle \Delta_{x1}(t)^2 \rangle \cong \langle \Delta_{y1}(t)^2 \rangle$, and the condition for mean *local* cylindrical symmetry is approximately satisfied for the bond vector $\mathbf{b}_1$, whose *local* "symmetry" axis is parallel to $\hat{\mathbf{z}}$, but perpendicular to the symmetry axis of the circle (i.e., $\hat{\mathbf{y}}$). This is what allows us to treat the rotational motions of each bond vector using the formulation developed for filaments with mean *local* cylindrical symmetry by taking the *local* symmetry axis, z_j, along the corresponding bond vector $\mathbf{b}_j$. As argued above, the bend in the line of bond vectors has only a slight effect on the local dynamics, which is then neglected under the assumptions made here.

References and Notes

(1) Schurr, J. M.; Fujimoto, B. S.; Wu, P.; Song, L. (1992) Fluorescence Studies of Nucleic Acids: Dynamics, Rigidities, and Structures. In *Topics in Fluorescence Spectroscopy, Vol. 3, Biochemical Applications* (Lakowicz, J. R., Ed.) Plenum Press: New York; pp 137−229.
(2) Thomas, J. C.; Schurr, J. M. *Biochemistry* **1983**, *22*, 6194−6198.
(3) Wilcoxon, J.; & Schurr, J. M. *Biopolymers* **1983**, *22*, 2273−2321.
(4) Robinson, B. H.; Lerman, L. S.; Beth, A.; Frisch, H. L.; Dalton, L. R.; & Auer, C. *J. Mol. Biol.* **1980**, *139*, 19−44.
(5) Millar, D. P.; Robbins, R. J.; & Zewail, A. H. *J. Chem. Phys.* **1982**, *76*, 2080−2094.
(6) Taylor, W. H.; & Hagerman, P. J. *J. Mol. Biol.* **1990**, *212*, 363−376.
(7) Wilcoxon, J.; Shibata, J. H.; Thomas, J. C.; & Schurr, J. M. (1982) in *Biomedical Applications of Laser Light Scattering* (Lee, W. I., Sattelle, D. B., Ware, B. R., Eds.) Elsevier Biomedical Press: Amsterdam; pp 27−36.
(8) Millar, D. P.; Ho, K. M.; & Aroney, A. J. *Biochemistry* **1988**, *29*, 799−811.
(9) Wu, P.; Song, L.; Clendenning, J. B.; Fujimoto, B. S.; Benight, A. S.; Schurr, J. M. *Biochemistry* **1988**, *27*, 8128−8144.
(10) Wu, P.; Schurr, J. M. *Biopolymers* **1989**, *28*, 1695−1703.
(11) Wu, P.; Fujimoto, B. S.; Song, L.; & Schurr, J. M. *Biophys. Chem.* **1991**, *41*, 217−236.
(12) Wu, P. (1988) Ph.D. Thesis, University of Washington.
(13) Fujimoto, B. S.; Shibata, J. H.; Schurr, R. L.; & Schurr, J. M. *Biopolymers* **1985**, *24*, 1009−1022.
(14) Fujimoto, B. S.; Schurr, J. M. *Nature* **1990**, *344*, 175−178.
(15) Kim, U. S.; Fujimoto, B. S.; Furlong, C. E.; Sundstrom, J. A.; Humbert, R.; Teller, D. C.; & Schurr, J. M. *Biopolymers* **1993**, *33*, 1725−1745.
(16) Shibata, J. H.; Wilcoxon, J.; Schurr, J. M.; & Knauf, V. *Biochemistry* **1984**, *23*, 1188−1194.
(17) Langowski, J.; Benight, A. S.; Fujimoto, B. S.; Schurr, J. M.; & Schomburg, U. *Biochemistry* **1985**, *24*, 4022−4028.
(18) Song, L.; Fujimoto, B. S.; Wu, P.; Thomas, J. C.; Shibata, J. H.; & Schurr, J. M. *J. Mol. Biol.* **1990**, *214*, 307−326.
(19) Clendenning, J. B.; Naimushin, A. N.; Fujimoto, B. S.; Stewart, D. W.; & Schurr, J. M. *Biophys. Chem.* **1994**, *52*, 191−218.
(20) Clendenning, J. B.; & Schurr, J. M. *Biopolymers* **1994**, *34*, 849−868.
(21) Shore, D., & Baldwin, R. L. *J. Mol. Biol.* **1983**, *170*, 957−981.
(22) Horowitz, D.; Wang, J. *J. Mol. Biol.* **1984**, *173*, 75−91.
(23) Heath, P. J.; Allison, S. A.; & Schurr, J. M. *SPIE* **1994**, *2370*, 294−301.
(24) Heath, P. J. (1995) Ph.D. Thesis, University of Washington.
(25) Chirico, G.; & Langowski, J. *Biopolymers* **1994**, *34*, 415−433.
(26) Schlick, T.; & Olson, W. K. *J. Mol. Biol.* **1992**, *223*, 1089−1119.
(27) Schurr, J. M.; & Fujimoto, B. S. *Biopolymers* **1988**, *27*, 1543−1569.
(28) Schurr, J. M. *Chem. Phys.* **1984**, *84*, 71−96.
(29) Ermak, D.; & McCammon, J. A. *J. Chem. Phys.* **1978**, *69*, 1352−1359.
(30) Allison, S. A.; & McCammon, J. A. *Biopolymers* **1984**, *23*, 363−375.
(31) Allison, S. A. *Macromolecules* **1986**, *19*, 118−123.
(32) Allison, S. A.; Austin, R. H.; & Hogan, M. E. *J. Chem. Phys.* **1989**, *90*, 3843−3854.
(33) Rotne, J.; & Prager, S. *J. Chem. Phys.* **1969**, *50*, 4831−4837.
(34) Yamakawa, H. *J. Chem. Phys.* **1970**, *53*, 436−443.
(35) Allison, S. A.; & McCammon, J. A. *Biopolymers* **1983**, *22*, 167−187.
(36) Iniesta, A.; Garcia de la Torre, J. *J. Chem. Phys.* **1990**, *92*, 2015−2018.
(37) Hao, M. H.; & Olson, W. K. *Macromolecules* **1989**, *22*, 3292−3303.
(38) Gebe, J. A.; Allison, S. A.; Clendenning, J. B.; & Schurr, J. M. *Biophys. J.* **1994**, *68*, 619−633.
(39) Allison, S. A.; & Schurr, J. M. *Chem. Phys.* **1979**, *41*, 35−59.
(40) Langowski, J.; Fujimoto, B. S.; Wemmer, D. E.; Benight, A. S.; Drobny, G.; Shibata, J. H.; & Schurr, J. M. *Biopolymers* **1985**, *24*, 1023−1056.
(41) Song, L.; Allison, S. A.; & Schurr, J. M. *Biopolymers* **1995**, *29*, 1773−1791.
(42) Hagerman, P. J.; & Zimm, B. H. *Biopolymers* **1981**, *20*, 1481−1502.
(43) Tirado, M. M.; & Garcia de la Torre, J. *J. Chem. Phys.* **1980**, *73*, 1986−1993.
(44) Wu, P.; Fujimoto, B. S.; & Schurr, J. M. *Biopolymers* **1987**, *26*, 1463−1488.
(45) Elias, J. G.; & Eden, D. *Macromolecules* **1981**, *14*, 410−419.
(46) Yamakawa, H.; Yamaki, J. *J. Chem. Phys.* **1973**, *58*, 2049−2055.
(47) Song, L.; & Schurr, J. M. *Biopolymers* **1990**, *30*, 229−237.
(48) Wu, J.; & Watts, R. O. *J. Chem. Phys.* **1995**, *103*, 3718−3732.
(49) Vologodskii, A. V.; & Cozzarelli, N. R. *Annu. Rev. Biophys. Biomol. Struct.* **1994**, *28*, 609−643.
(50) Edmonds, A. R. (1974) *Angular Momentum in Quantum Mechanics*; Princeton University Press: Princeton, NJ.
(51) Fujimoto, B. S.; Miller, J. M.; Ribeiro, N. S.; & Schurr, J. M. *SPIE Proc.* **1993**, *1922*, 360−367.
(52) Ramachandran, G.; Schlick, T. *Phys. Rev. E* **1995**, *51*, 6188−6203.
(53) Ramachandran, G.; Schlick, T. Beyond optimization: simulating the dynamics of supercoiled DNA by a macroscopic model. DIMACS Series in Discrete Mathematics and Theoretical Computer Science, in press.

MA951167T